

Moving Particle Semi-implicit method coupled with Finite Element Method for hydroelastic responses of floating structures in waves

Guanyu Zhang, Weiwen Zhao, Decheng Wan*

Computational Marine Hydrodynamics Lab (CMHL), School of Naval Architecture, Ocean and Civil Engineering, Shanghai Jiao Tong University, Shanghai 200240, China

ARTICLE INFO

Article history:
Available online 18 April 2022

Keywords:
Moving Particle Semi-implicit (MPS)
MPS–FEM coupled method
Wave–Structure Interaction (WSI)
Flexible ship

ABSTRACT

In this paper, the Moving Particle Semi-implicit (MPS) method and Finite Element Method (FEM) coupling computational method is applied to solve the problem of hydroelastic response of floating structures. The MPS method, a Lagrangian meshfree method, is suitable for simulating violent flows such as breaking waves on free surface. For a floating structure like the ship hull and floating breakwater, the typical feature of motion is a large rigid-body motion plus a relatively small deformation. Therefore, a rigid–flexible coupling strategy based on MPS–FEM coupled method is developed. According to the choice of structural element, appropriate data transformation schemes are adopted on the fluid–structure interface. In this paper, the grouping exchange technique is developed, which is applied on the interface of particle model–beam element. The reliability of present method is verified through simulations of fluid–structure interaction (FSI) problems including water entry of the elastic wedge, water entry of the marine panel and dam-break wave impacting on a mooring flexible platform, the obtained numerical result is in good agreement with the published data. Afterwards, the coupling of fluid and structure solver is also tested by various problems including the cases of three-dimensional deformable floating platform/ship slamming in waves.

© 2022 Elsevier Masson SAS. All rights reserved.

1. Introduction

Wave-induced motions and structural deformations are common and interesting fluid–structure interaction (FSI) problems in the field of marine and offshore engineering, and their great complexity concerns the violent free surface and nonlinear structural deformation and vibration. On the one hand, for the marine vessels, offshore structures, and so on, while encountering extreme conditions, there will be elastic vibration even fatigue damage which would bring new challenges for the structural security. On the other hand, the wave-induced structural response could significantly influence the evolution of the free surface.

Increasingly numerous diverse computational methods have been developed for the Wave–Structure Interaction (WSI) problems. Mesh-based approaches, such as the Finite Element Method (FEM) [1], the immersed boundary method (IBM) [2,3], and Lattice Boltzmann method (LBM) [4,5], have been widely applied for the WSI problems. Shen et al. [6] employed dynamic overset grid technology to analyze the motion response of KCS model with rotating propeller in head waves based on open-source platform OpenFOAM. Lakshmyanarayana and Temarel [7,8] established the cosimulation between Finite Volume Method (FVM) and FEM

through the software of Star-CCM+ and Abaqus with the overset grid to investigate the motion and deformation of a flexible barge in the regular wave. Nevertheless, remeshing may introduce an undesired diffusivity, thus reducing robustness and accuracy [9]. In this regard, a more suitable computational method in modeling FSI problems with free surfaces motion and significant movement and deformation of structures is desirable.

Unlike the grid-based methods, particle-based methods are inherently Lagrangian methods, which can deal with the large deformation and strong nonlinear phenomenon of free surfaces relatively more straightforward [10,11], as well as the moving boundaries. Therefore, particle-based methods have been intensely studied over the past decades, including Smoothed Particle Hydrodynamics (SPH) [12], Moving Particle Semi-implicit method (MPS) [13], and Material Point Method (MPM) [14]. Numerous good works have proved the ability of particle-based methods in simulating free-surface flows and achieved good achievements, such as the dam-break flow [15–17], the water entry problems [18–20], the liquid sloshing [21–24], and so on. Recently, some studies have been conducted on implementation of these Lagrangian particle methods into WSI problems. Sueyoshi et al. [25] simulated the two-dimensional wave-induced nonlinear motions of a floating body by MPS method. Shibata et al. [26] simulated the three-dimensional ship motion with a forward speed under high wave height conditions. The potential of the

* Corresponding author.
E-mail address: dcwan@sjtu.edu.cn (D. Wan).

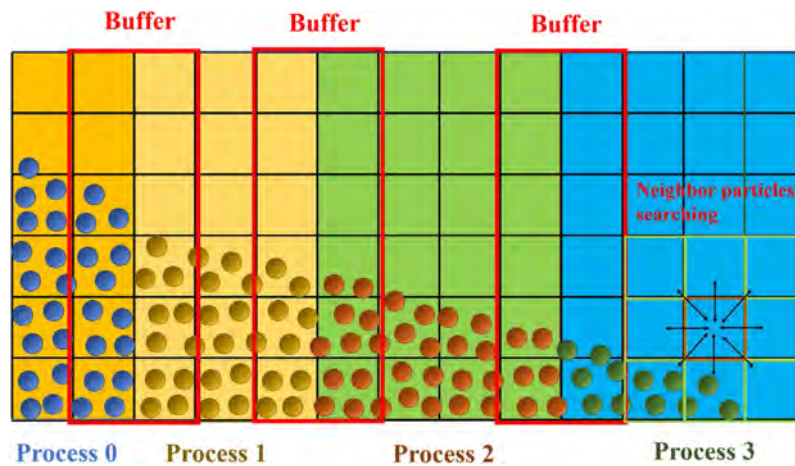


Fig. 1. Schematic diagram of parallel computing based on MPI.

MPS method as a new simulation tool can be proved. Guo et al. [27] simulated water flooding of a damaged floating structure through three-dimensional SPH method. Kawamura et al. [28] simulated the water-shiping problems through the SPH method to investigate the 6Dof motion of the ship model under the condition of the following wave and stern quartering wave. Ni et al. [29] developed a novel numerical wave–current flume based on SPH method to investigate the wave–current interaction.

More recently, particle-based methods have been coupled with other methods to model fluid–structure interaction (FSI) problems involving structural deformation [30,31], such as MPS–FEM [32–36], SPH–FEM [37–39], MPS–Discrete Element Method (MPS–DEM) [40,41], MPS–mode superposition method [42,43], SPH–Total Lagrangian Particle (SPH–TLP) [44–46], and ISPH–SPH [47], multi-resolution MPS–MPS [48], multi-resolution SPH [49–51], SPH–smoothed finite element method (ES–FEM) [52], and SPH–Hamiltonian SPH (HSPH) [53]. Some researchers investigated the energy conservation properties of coupled methods [41,47,54], the results show that the energy conservation properties of coupled methods are acceptable. In this paper, the MPS–FEM coupled model is applied for FSI problems, in which the MPS method is used for the simulation of violent free-surface flow of fluids. In addition, FEM has its robustness and accuracy in the solving of structural deformation.

In the aforementioned research, the deformable structures are mostly ended fixed, displaying elastic deformation only without movement. For a floating structure like the ship hull and floating breakwater that sustain wave-induced force or others, the typical motion feature is a large rigid-body motion plus a relatively small deformation. A computational model that coupled rigid-body motion and elastic deformation is needed in WSI analyses. Khayyer et al. [47,53] simulated the water entry problem of an elastic wedge with high velocity using ISPH–SPH and ISPH–HSPH method. Sun et al. [40] investigated the motion of a two-dimensional mooring floating flexible platform under dam-break wave impacting through MPS–DEM coupled method. Sun et al. [43] simulated the three-dimensional ship hull slamming in the wave through the coupled MPS–modal superposition method. The ship hull is simplified as the non-uniform beam. The motion of the ship was described by the Coupled Rigid-body and Flexible mode (CRF) model based on modal superposition method. As a reference, a computational model which couples the rigid-body motion and elastic deformation based on MPS–FEM coupled method is developed to simulate the hydroelastic response of floating structures in waves.

In this paper, a computational model which couples the MPS method for fluid field and FEM for structure field is developed

to investigate the hydroelastic response of floating structures in waves. In our previous researches, the MPS method was modified to improve the accuracy of pressure computation and stability [16,55–59]. Based on this, a rigid–flexible coupling strategy based on MPS–FEM coupled method is developed in this paper for the deformable floating structures. On the fluid–structure interface, appropriate data transformation scheme is adopted according to the dispersed structural element. For instance, Shape Function Based Interpolation Technique (SFBI) is applied on the interface of particle model–solid element [36]. For the interface of particle model–beam element, grouping exchange technique is developed. An accelerated computing technique of the multi-CPU parallel technique is used to improve the computation efficiency. The rest of the paper is arranged as follows: Section 2 introduces the MPS method and FEM method briefly, as well as the rigid–flexible coupling strategy. Afterwards, the coupling scheme between fluid and solid solver and the data transformation scheme on the fluid–structure interface will be introduced. In Section 3, the reliability and accuracy of proposed model are validated through the case of hydroelastic slamming of an elastic wedge, hydroelastic slamming of the marine panel and dam-breaking wave impacting on a deformable mooring platform. The comparisons between the present numerical results and published data [40,60,61] are conducted. In Section 4, the coupling of fluid and structure solver is also tested by various problems, including the cases of the three-dimensional deformable floating box/ship slamming in waves.

2. Numerical method

In this study, the partitioned MPS–FEM method is adopted to investigate the FSI problems. The MPS method is used to calculate the fluid field, while the FEM is adopted to solve the structure field for coupling the rigid-body motion plus elastic deformation. The theories for the MPS have been presented with details in our previous papers [16,33,55–59], which are introduced briefly in this section. Afterwards, the model of the rigid–flexible coupling strategy based on FEM, the coupling scheme between MPS method and FEM method, as well as the data transformation scheme on the fluid–structure interface will be introduced in detail.

2.1. MPS formulation for fluid dynamics

The governing equations for the viscous incompressible fluid mainly include the continuity equation and momentum equation, which are expressed in Lagrangian form as following,

$$\nabla \cdot \mathbf{V} = 0 \quad (1)$$

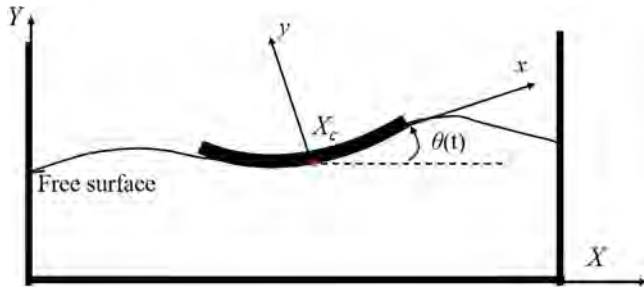


Fig. 2. The flexible beam element deformation.

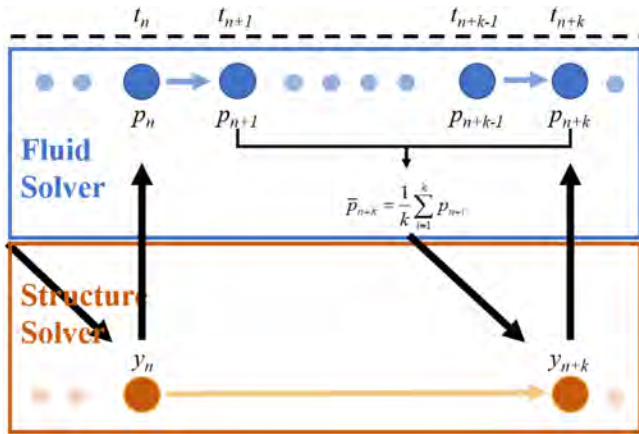


Fig. 3. Schematic diagram of coupling strategy between fluid and structure field.

$$\frac{D\mathbf{V}}{Dt} = -\frac{1}{\rho}\nabla p + \nu\nabla^2\mathbf{V} + \mathbf{g} \quad (2)$$

where ρ and ν denote the fluid density and kinematic viscosity, \mathbf{V} , ∇p , and \mathbf{g} present the velocity vector, the pressure gradient, and the gravitational acceleration.

In the MPS method, the kernel function $W(r)$ acts as the weight function in the discretization process and determine the interaction between particles, written as,

$$W(r) = \begin{cases} \frac{r_e}{0.85r + 0.15r_e} - 1 & 0 \leq r < r_e \\ 0 & r_e \leq r \end{cases} \quad (3)$$

where $r = |\mathbf{r}_j - \mathbf{r}_i|$ is the distance between particle i and j , and r_e denotes the influence radius of the target particle. The adopted kernel function can avoid the non-physical pressure oscillation and improve the computational stability.

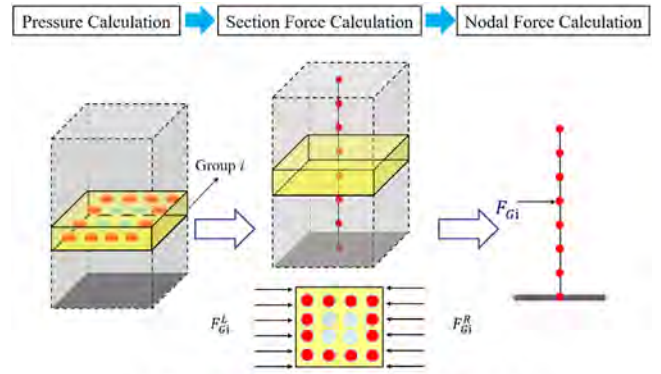
Models of particle interaction include gradient model, divergence model, and Laplacian model. These models can be written as,

$$\langle \nabla \phi \rangle_i = \frac{D}{n^0} \sum_{j \neq i} \frac{\phi_j + \phi_i}{|\mathbf{r}_j - \mathbf{r}_i|^2} (\mathbf{r}_j - \mathbf{r}_i) \cdot W(|\mathbf{r}_j - \mathbf{r}_i|) \quad (4)$$

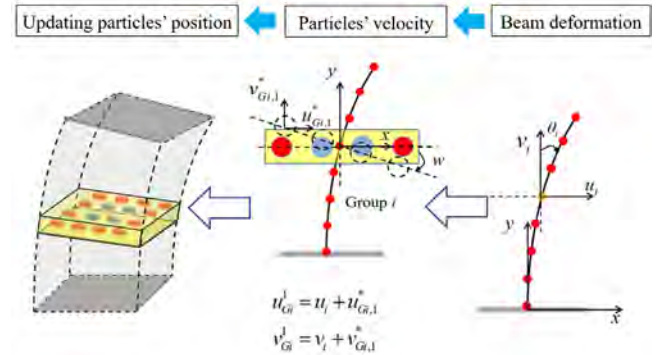
$$\langle \nabla \cdot \Phi \rangle_i = \frac{D}{n^0} \sum_{j \neq i} \frac{(\Phi_j - \Phi_i) \cdot (\mathbf{r}_j - \mathbf{r}_i)}{|\mathbf{r}_j - \mathbf{r}_i|^2} W(|\mathbf{r}_j - \mathbf{r}_i|) \quad (5)$$

$$\langle \nabla^2 \phi \rangle_i = \frac{2D}{n^0 \lambda} \sum_{j \neq i} (\phi_j - \phi_i) W(|\mathbf{r}_j - \mathbf{r}_i|) \quad (6)$$

where ϕ is a scalar function, like the pressure p . Φ presents a vector, like the velocity \mathbf{V} . D is the number of space dimensions, r is the position vector, λ is a parameter and expressed as Eq. (7),



(a) The force equivalence condition



(b) The displacement equivalence condition

Fig. 4. Concepts of three-dimensional grouping exchange technique.

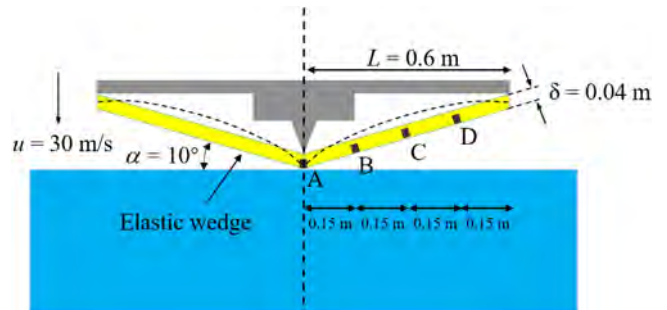


Fig. 5. Geometric model of the elastic wedge on the still free surface.

and n^0 is the initial density of the particle number.

$$\lambda = \frac{\sum_{j \neq i} W(|\mathbf{r}_j - \mathbf{r}_i|) |\mathbf{r}_j - \mathbf{r}_i|^2}{\sum_{j \neq i} W(|\mathbf{r}_j - \mathbf{r}_i|)} \quad (7)$$

The pressure is calculated by solving the Pressure Poisson Equation (PPE). A mixed source term method, proposed by Tanaka [62] and Lee [63], is applied in the present solver, which combines the velocity divergence-free condition and constant particle number density condition.

$$\langle \nabla^2 p^{k+1} \rangle_i = (1 - \gamma) \frac{\rho}{\Delta t} \nabla \cdot \mathbf{V}_i^* - \gamma \frac{\rho}{\Delta t^2} \frac{\langle n^k \rangle_i - n^0}{n^0} \quad (8)$$

where p_{k+1} , Δt and \mathbf{V}_i^* are the pressure of the step $k + 1$, time step and temporal velocity. γ is the weight of the particle number

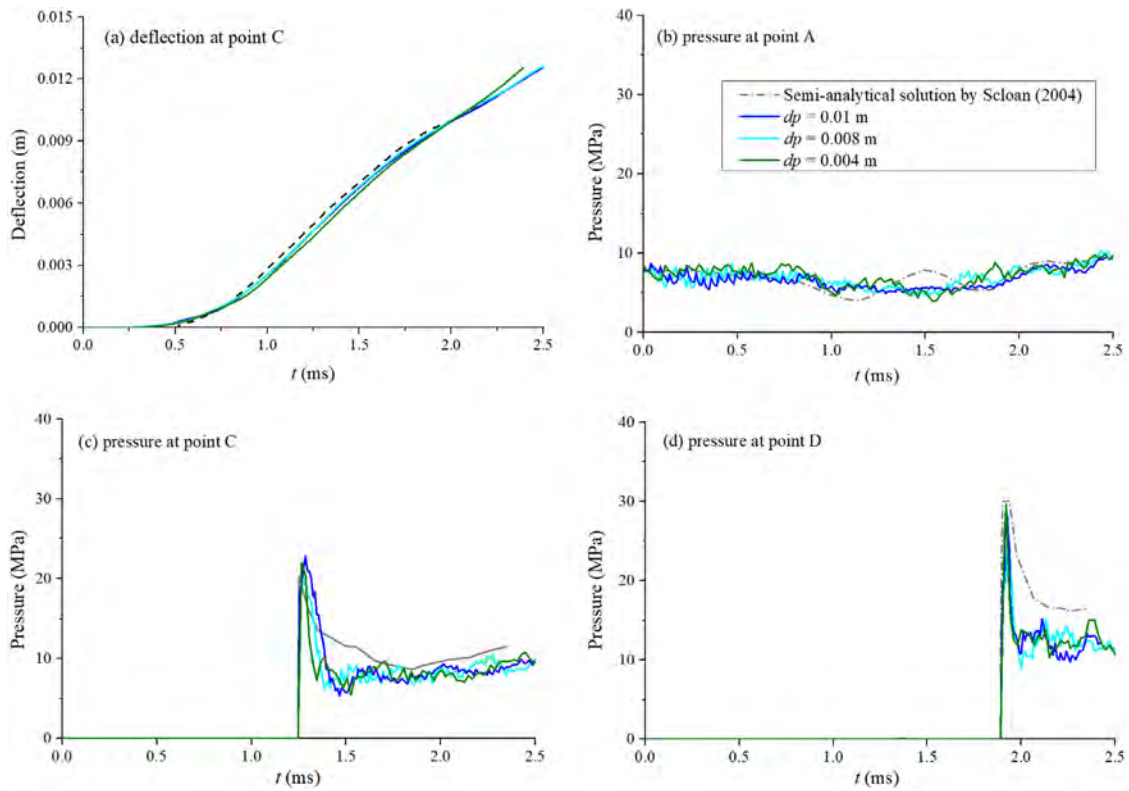


Fig. 6. Time histories of (a) deflection at point C and (b–d) pressure at points A, C and D with corresponding semi-analytical solutions [60].

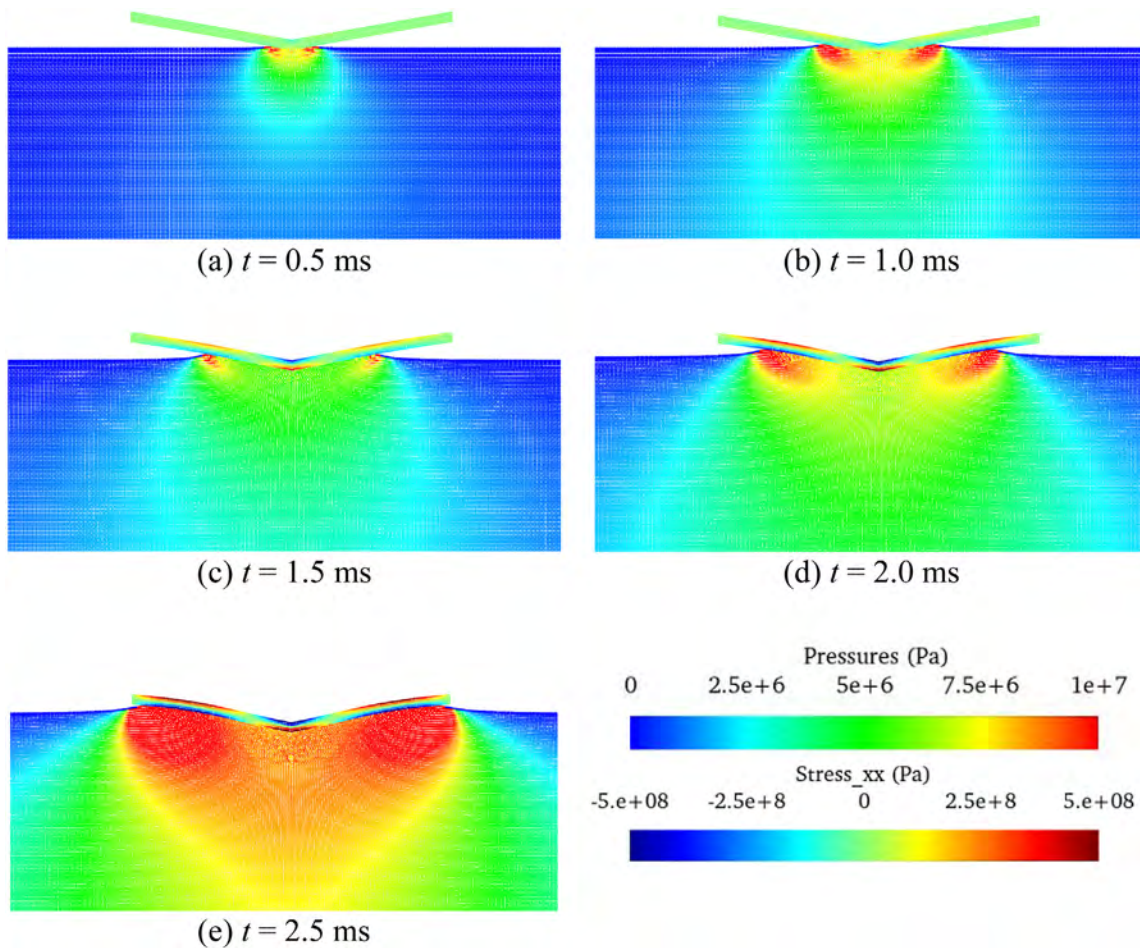


Fig. 7. The pressure/stress fields during the elastic wedge impacting still free surface.

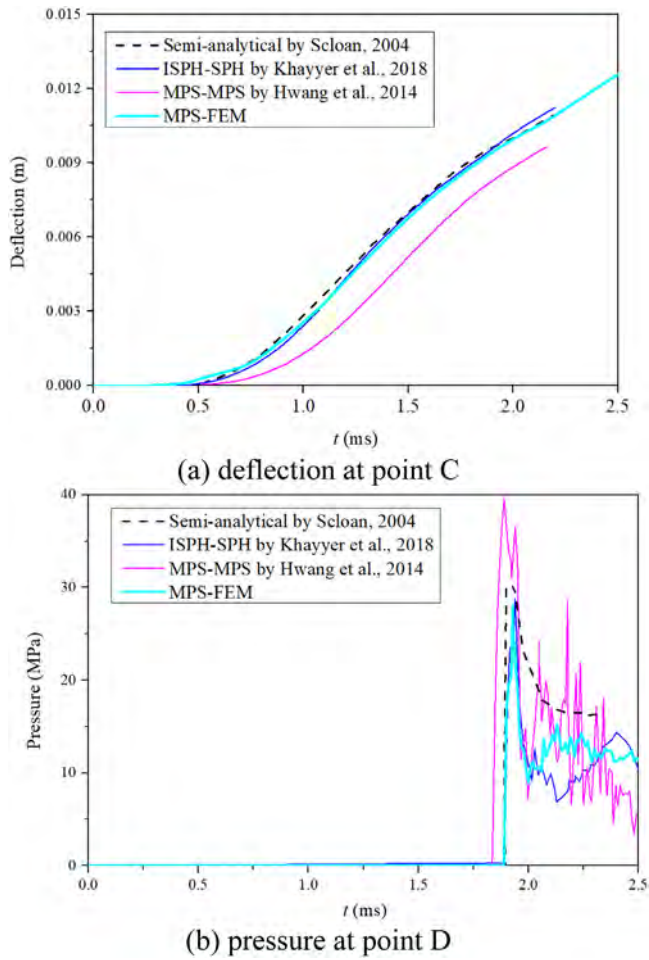


Fig. 8. Quantitative comparisons of MPS-FEM coupled method with MPS-MPS method [65] and ISPH-SPH [47] method, in terms of deflection (a) and pressure (b).

density term between 0 to 1. In this paper, $\gamma = 0.01$ is adopted throughout all simulations. n^k is the temporal particle number density at k step and defined as,

$$\langle n^k \rangle_i = \sum_{j \neq i} W(|\mathbf{r}_j - \mathbf{r}_i|) \quad (9)$$

The detection of free surface particle is of importance in computational accuracy and stability. In the present paper, we employ an improved free surface particle detection method by Zhang et al. [55] and Khayyer et al. [64] and defined as,

$$\langle n^k \rangle_i / n^0 < \beta \quad (10)$$

$$\begin{cases} \langle \mathbf{F} \rangle_i = \frac{D}{n^0} \sum_{j \neq i} \frac{(\mathbf{r}_j - \mathbf{r}_i)}{|\mathbf{r}_j - \mathbf{r}_i|} W(|\mathbf{r}_j - \mathbf{r}_i|) \\ \langle \mathbf{F} \rangle_i > \alpha |\mathbf{F}|^0 \end{cases} \quad (11)$$

where $\langle \mathbf{F} \rangle_i$ represents the asymmetric arrangements of neighbor particles, and $|\mathbf{F}|^0$ is the initial value of $\langle \mathbf{F} \rangle_i$ for surface particles. The parameters β and α are set to 0.8 and 0.9, respectively.

In general, when particles get close to each other, the repulsive force between particles will be generated to avoid the clusters of particles. However, it is inevitable for the particle collection in strong nonlinear flow. Therefore, collision model is adopted in this paper, which was originally proposed by Koshizuka et al. [66] and Lee et al. [63]. In present MPS method, when the distance between two particles is less than $\alpha * l_0$, the collision model will

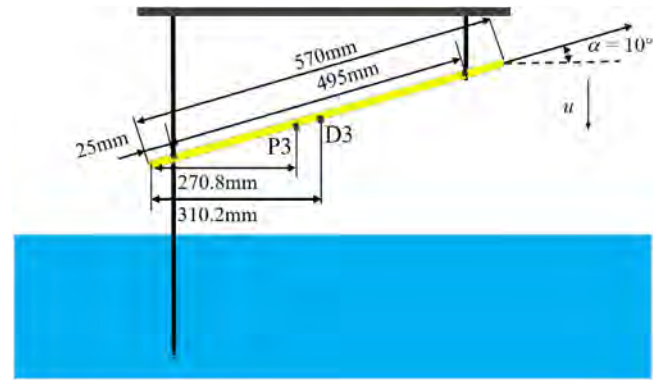


Fig. 9. Geometric model of the marine panel impacting the still free surface.

be applied. The parameter α is set to 0.8 in this paper. The correction of particles' velocities will follow the linear momentum conservation law and defined as,

$$\mathbf{u}'_i = \mathbf{u}_i - (1 + \varepsilon) \mathbf{u}_{ij}^n \quad (12)$$

$$\mathbf{u}'_j = \mathbf{u}_j + (1 + \varepsilon) \mathbf{u}_{ij}^n \quad (13)$$

where \mathbf{u}_{ij}^n is the relative velocity of particle i and j along the normal direction. ε is the collision coefficient, which is set as 0.5 in this paper.

In the simulation of three-dimensional FSI problems, the large amount of computation is considerable challenge, such as the neighborhood particles searching and PPE solving. It is difficult for serial programs to perform such large-scale simulations. In this paper, the CPU parallel acceleration technology based on Message Passing Interface (MPI) is adopted. Firstly, the background grid [67] is introduced to provide the reference frame for neighbor particles searching. Then the computing domain will be divided into a certain number of subdomains according to the background grid, as shown in Fig. 1, each process in MPI is responsible for the computation of one subdomain. The size of each subdomain is variable to make sure the particle numbers in each subdomain remain approximately constant. The grid adjacent to other processes is called buffer. In the buffer, the information will be exchanged between adjacent processes. It should be noted that the present method runs on the High-Performance Computing (HPC) cluster of CMHL group (CPU of Intel Xeon E5-2680 v2 10 Cores \times 2.80 GHz/node and RAM 64 GB).

2.2. FEM formulation for rigid-flexible coupling motion

For a floating structure like the ship hull and floating breakwater, the typical motion feature is a sizeable rigid-body motion plus a relatively small deformation. In this section, a rigid-flexible coupling strategy based on FEM is introduced, which couples the rigid-body motion and flexible deflection. For the flexible deformation, according to the theory of FEM, the dynamic balance equation of nodes after the structure is discretized can be written as follows:

$$\mathbf{M}\ddot{\mathbf{u}} + \mathbf{C}\dot{\mathbf{u}} + \mathbf{K}\mathbf{u} = \mathbf{F} \quad (14)$$

$$\mathbf{C} = \alpha \mathbf{M} + \beta \mathbf{K} \quad (15)$$

where \mathbf{M} , \mathbf{C} and \mathbf{K} represent the mass matrix, Rayleigh damping matrix and stiffness matrix of the structure analysis. $\mathbf{F}(t)$ is the force vector of the structure and varies with computational time. For simplicity of implementation, the Rayleigh damping is used, damping matrix \mathbf{C} is assumed to be a linear combination of \mathbf{M} and \mathbf{K} , where β_1 and β_2 are the Rayleigh damping coefficients.

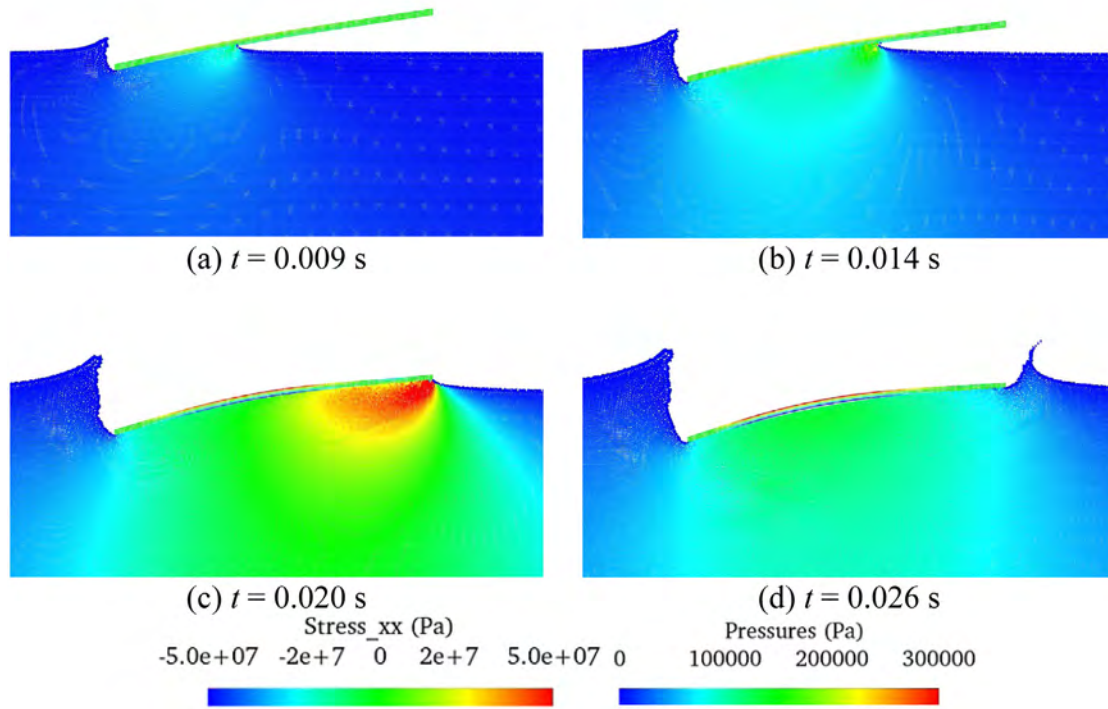


Fig. 10. Hydroelastic slamming of the marine panel ($u = 4.0$ m/s)

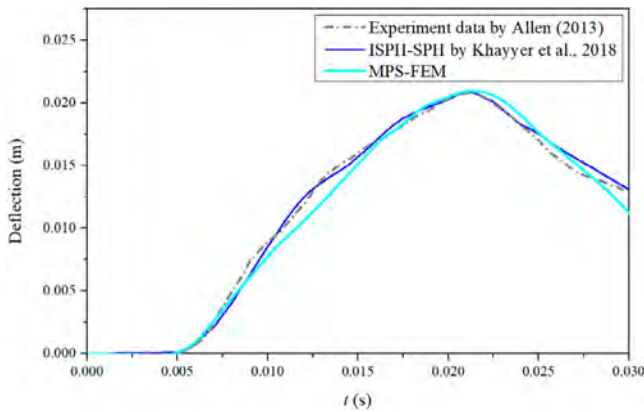


Fig. 11. Time history of the deflection at point D3 for the velocity of $u = 4$ m/s.

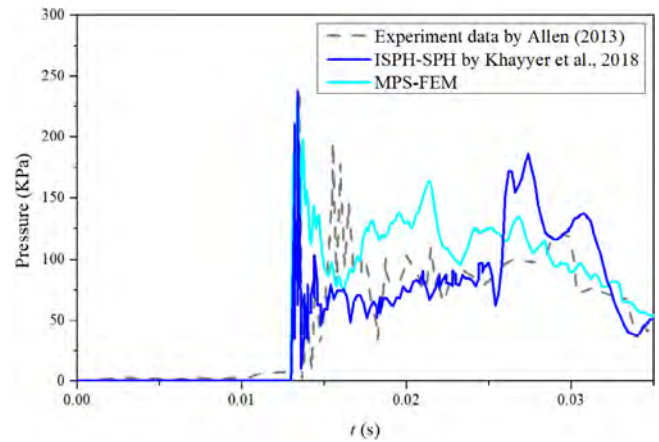


Fig. 12. Time history of the pressure at point P3 for the velocity of $u = 3$ m/s.

The choice of the time integration scheme is a key point in FEM, in this study, the Newmark- β method [68] is used. In a three-dimensional structure model, the structural matrix is a large-scale symmetric sparse matrix. In the present paper, the compressed sparse row (CSR) format is used for storing the large-scale symmetric sparse matrix, and the Biconjugate gradient stabilized algorithm (BiCGSTAB) is applied for solving the linear algebraic equation.

To solve the rigid-body motion coupled with flexible deformation, two coordinate systems are used here, fixed global system $X-Y$ and body-attached local system $x-y$, as shown in Fig. 2. As a result, the position of floating structure can be described as,

$$\mathbf{X} = \mathbf{X}_c + \mathbf{A}\mathbf{x} \tag{16}$$

where \mathbf{X}_c and \mathbf{A} are related to the rigid motion of floating structure. \mathbf{X}_c is the center position of the floating structure in global fixed system $O-XY$. \mathbf{A} denotes the transformation matrix from

local body-attached system $o-xy$ to global fixed system $O-XY$, which can be expressed as,

$$\mathbf{A} = \begin{bmatrix} \cos \theta & -\sin \theta \\ \sin \theta & \cos \theta \end{bmatrix} \tag{17}$$

Extending the model to three-dimensional case, the transformation matrix \mathbf{A} can be written as,

$$\mathbf{A} = \begin{bmatrix} \cos \beta \cos \theta & \cos \beta \sin \theta & -\sin \beta \\ \sin \alpha \sin \beta \cos \theta - \cos \alpha \sin \theta & \sin \alpha \sin \beta \sin \theta + \cos \alpha \cos \theta & \sin \alpha \cos \beta \\ \cos \alpha \sin \beta \cos \theta + \sin \alpha \sin \theta & \cos \alpha \sin \beta \sin \theta - \sin \alpha \cos \theta & \cos \alpha \cos \beta \end{bmatrix} \tag{18}$$

where the Euler angle between the global fixed system $O-XYZ$ and local body-attached system $o-xyz$ can be written as $[\alpha, \beta, \theta]^T$.

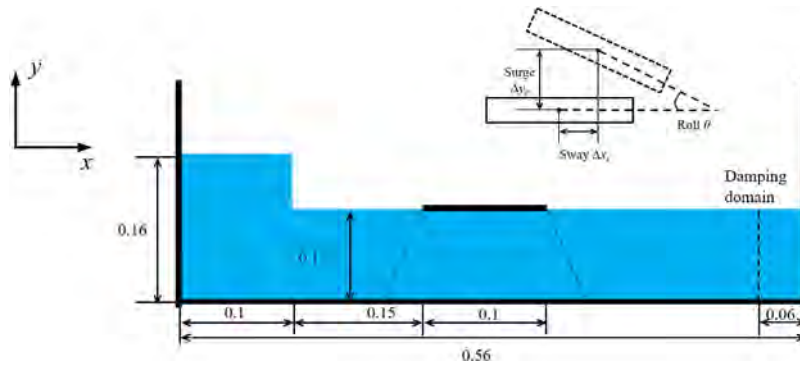


Fig. 13. Geometric model of the numerical wave tank.

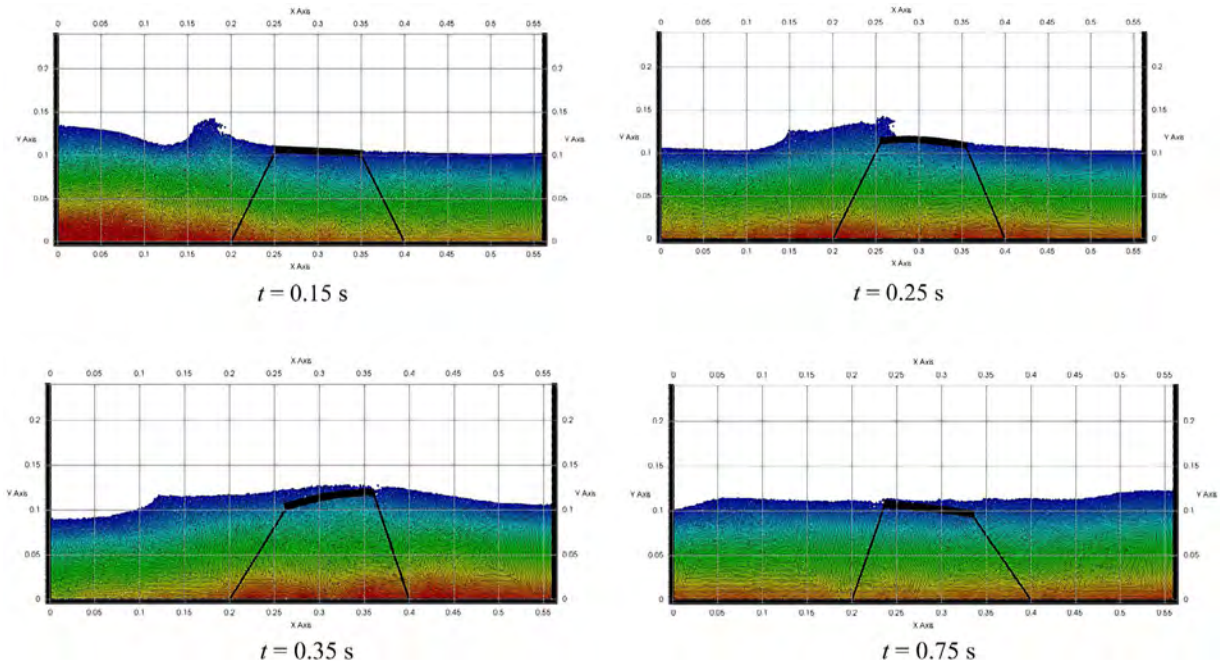


Fig. 14. The process of dam break flow impacting on a deformable platform.

The equations of rigid body dynamics are used for solving rigid floating bodies in the global X-Y system,

$$\mathbf{F}_e = m\mathbf{g} + \int p dS \quad (19)$$

$$\mathbf{M}_e = r_{cg} \times m\mathbf{g} + \int \mathbf{r} \times p dS \quad (20)$$

where m is the mass of the floating structure, r_{cg} represents the distance from the center of rotation to the center of gravity. The subscript e represents the global coordinate system. Further, the rigid body motion in the translational and rotational degrees of freedom are given. \mathbf{x} is the position corresponding to the local body-attached system x - y , which can be defined as,

$$\mathbf{x} = \mathbf{r}_0 + \mathbf{v} \quad (21)$$

\mathbf{r}_0 and \mathbf{v} present the position of any point in floating structure and elastic deformation in the local body-attached system x - y , respectively. The elastic deformation can be described based on FEM theory,

$$\mathbf{v} = \mathbf{N}\mathbf{u} \quad (22)$$

where \mathbf{u} denotes the node displacement and \mathbf{N} is the shape function in the FEM method. By this means, the rigid motion and elastic deformations can be considered at the same time.

2.3. MPS-FEM coupled scheme

In this study, a weak coupling strategy between MPS and FEM method is implemented. The traditional Conventional Serial Staggered (CSS) strategy is employed for the partitioned coupling approach, as shown in Fig. 3. And the interaction procedure can be summarized as follows:

(1) The pressure of the boundary particle is obtained at each fluid time step. Then the pressure should be averaged during Δt_s , to obtain the external force on the element node, as follows:

$$\bar{p}_{n+1} = \frac{1}{k} \sum_{i=1}^k p_{n+i} \quad (23)$$

where p_{n+1} is the pressure of the fluid particle on the boundary at $t + i\Delta t_f$, and \bar{p}_{n+1} is the average pressure of the fluid particle within Δt_s .

(2) The external force vector $\mathbf{F}_{t+\Delta t_s}$ of the structural boundary particles is calculated by multiplying the average pressure p_{n+1}

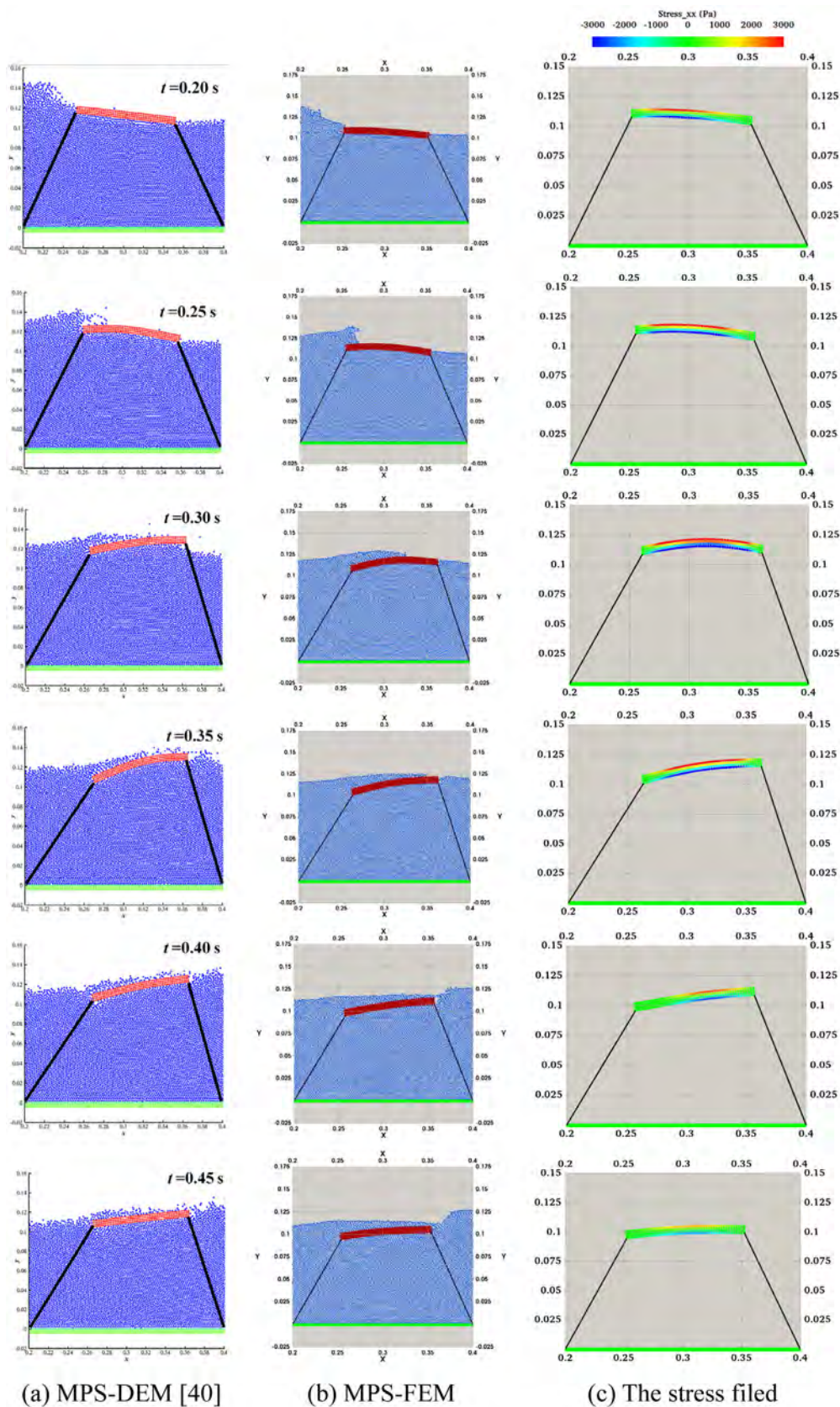


Fig. 15. Comparison between the published data [40] and MPS-FEM simulation results.

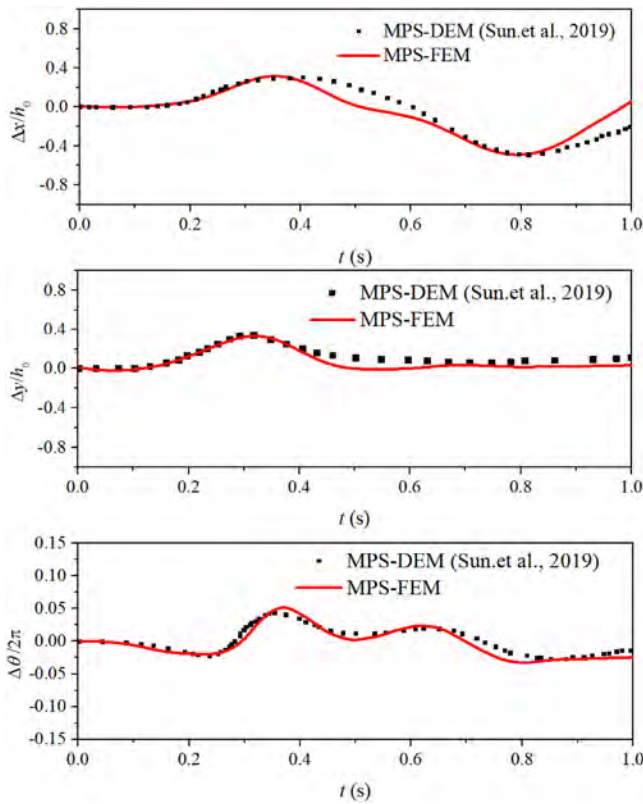


Fig. 16. The dimensionless surge, heave, and pitch responses of the deformable floating platform.

and the influential area, which equals the square of the initial particle spacing dp .

$$\mathbf{F}_{t+\Delta t_s} = \bar{p}_{n+1} \cdot dp \cdot dp \quad (24)$$

(3) The structural nodal displacements and velocities at the next structural time step can be calculated through solving the structural dynamic equations.

(4) Update the velocity and position of the structural boundary particles at each structural time step and the fluid particles at each fluid time step.

2.4. Data exchange on the fluid–structure interface

In this paper, the fluid domain is dispersed as particles and the structure is dispersed as beam elements or solid elements. Therefore, special schemes are required for data transformation on the fluid–structure interface, including applying the external force carried by the fluid particles onto the structure nodes and updating the position of boundary particles corresponding to the nodal displacements. More specifically, the displacement equivalence condition and the force equivalence condition must be satisfied. According to the choice of structural element, such as beam element and solid element, appropriate data transformation schemes are adopted on the fluid–structure interface. On the interface of particle model–solid element, the Shape Function Based Interpolation Technique (SFBI) was proposed [36], which will be applied in present paper. In this paper, grouping exchange technique on the interface of particle model–beam element will be developed, as shown in Fig. 4. Different form Zhang and Wan [57] and Hwang et al. [69], the proposed data exchange technique can be extended to three-dimensional interface. The boundary particles located at the same section are divided into

the same group, and each group regards as a node of the beam element. The concept of the force transformation is shown in Fig. 4(a), where the vectors represent the force acting on the left and right boundary particle of the structural group i . As stated above, the pressure of boundary particle is calculated through PPE. Then, the force acting on the structural boundary particle is calculated by the integration of the average pressure acting on the interface. Afterwards, the resultants within the same group are applied onto the structural node as the external force for the structural physics analysis. For the velocity, the velocity of structure particles is equal to the velocity of structure boundary at the interface. Particles within a group move as a unit according to the nodal linear velocities and angular velocity. The concept of the velocity transformation is shown in Fig. 4(b).

3. Validation

The MPS–FEM coupled method was validated through several FSI benchmarks, such as dam break flow slamming on the elastic flap and liquid sloshing flow with elastic baffle [36]. The numerical results confirm that the coupled method has capable of simulating the fluid–structure interaction. In this paper, the performance of the MPS–FEM coupled method is evaluated in simulations of hydroelastic responses of floating structures, including hydroelastic slamming of an elastic wedge [60], hydroelastic slamming of the marine panel [61] and dam-breaking wave slamming on a deformable mooring platform [40].

3.1. Water entry of the elastic wedge

In this section, the hydroelastic behavior of a high-speed impact of an elastic wedge on the still free surface is investigated, where the semi-analytical solutions are provided by Scolan [60]. The elastic wedge is 0.6 m in length and 0.04 m in thickness, and the wedge impacts the free surface with a dead-rise angle of $\alpha = 10^\circ$, the geometric model is shown as Fig. 5. The wedge falls down with a constant vertical velocity of $u = 30.0$ m/s. The density of structure is $\rho_s = 2700$ kg/m³, and Young's modulus is $E_s = 67.5$ GPa. The convergence study is carried out to verify the solver's stability. The particle spacings are $dp = 0.01$ m, 0.008 m and 0.004 m, respectively. The numbers of particles are 37 710, 58 546 and 231 106, respectively. The time step is set as $\Delta t = 1.0E-5$ s. 4 CPU cores are used in this case.

Time histories of the deflection at point C and the pressure at points A, C and D by the MPS–FEM coupled method with three particle resolutions are presented in Fig. 6. According to this figure, the results under different resolutions are almost equivalent and agree relatively well with the semi-analytical solutions by Scolan [60], especially the deflection at point C. The error analysis of the pressure peak compared with the experiment data at points A, C and D is shown in Table 1, under three particle resolutions. From the presented results, the MPS–FEM coupled solver is shown to possess proper convergence properties. The particle spacing $dp = 0.008$ is therefore used in the following simulations.

Fig. 7 illustrates snapshots of pressure/stress fields at $t = 5.0$ ms, 10.0 ms, 15.0 ms, 20.0 ms and 25.0 ms. Once the elastic wedge impacts on the still free surface, the relatively obvious slamming pressure can be observed, the midspan of the wedge therefore has an upward deflection. From the figure, the stability of the present MPS–FEM coupled solver is well depicted according to smoothness of pressure and stress fields.

Fig. 8 presents quantitative comparisons corresponding to the deflection at point C the pressure at point D, between numerical results by present MPS–FEM coupled solver and those by MPS–MPS method [65] and ISPH–SPH method [47]. It can be seen that

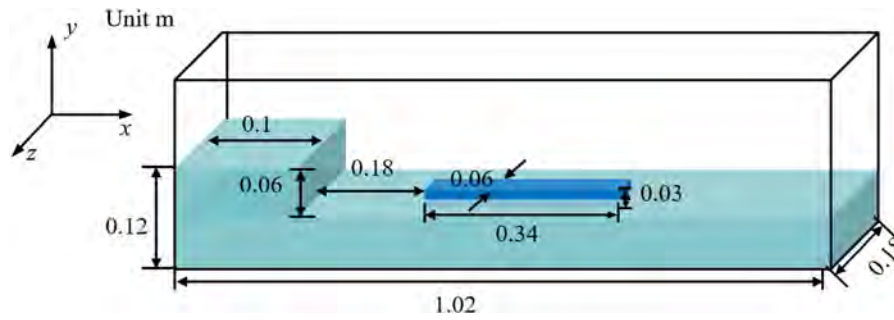


Fig. 17. The numerical geometric model of dam-break wave impacting on the floating structure.

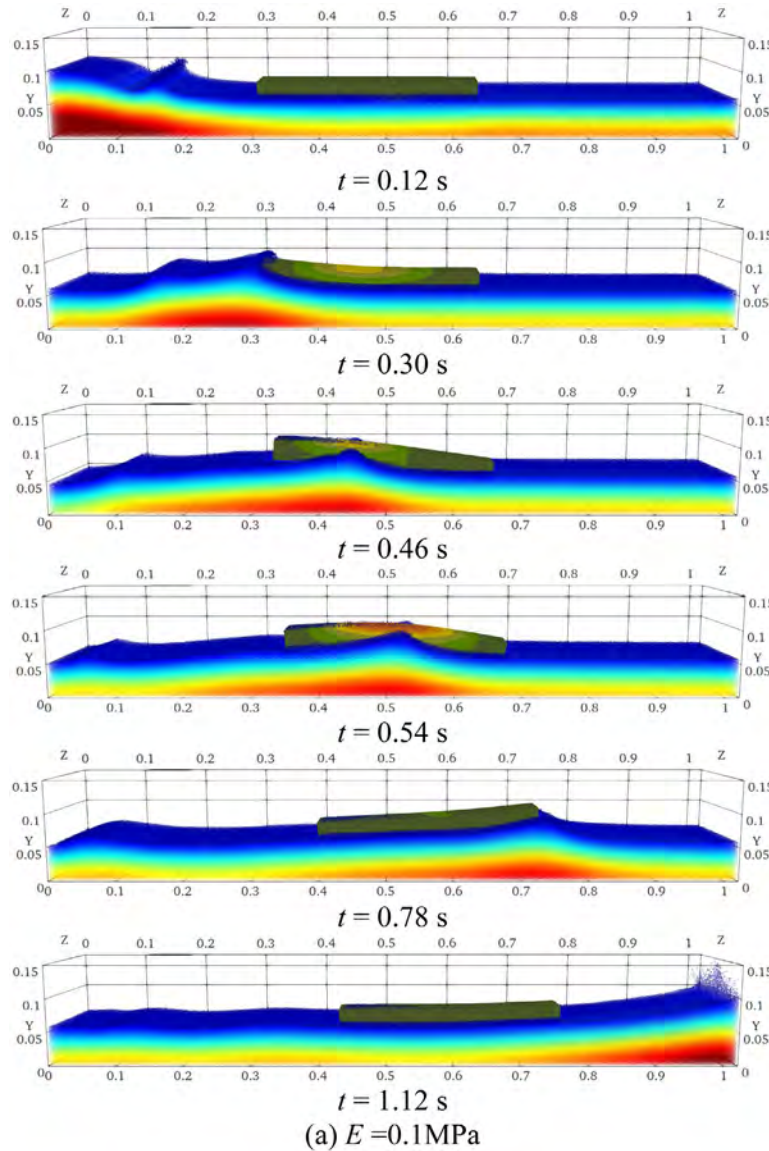


Fig. 18. The motion and deformation of the floating structure.

the proposed method shows good consistency among various approaches.

3.2. Hydroelastic slamming of the marine panel

In this section, MPS–FEM coupled method is further validated through the simulations of hydroelastic slamming of the marine

panel, where the experimental result was provided by Allen [61]. The geometric model is shown as Fig. 9. The marine panel is a Solid Glass (SG)-fiber single skin panel, with 1.03 m in length, 0.6 m in width and 0.0095 m in thickness. The bending stiffness and shear stiffness are set as 1520 Nm and 44 000 kN/m, respectively. The mass of the panel is set as 18.3 kg/m². The both edges of the panel are simply supported by the fixture frame, setting

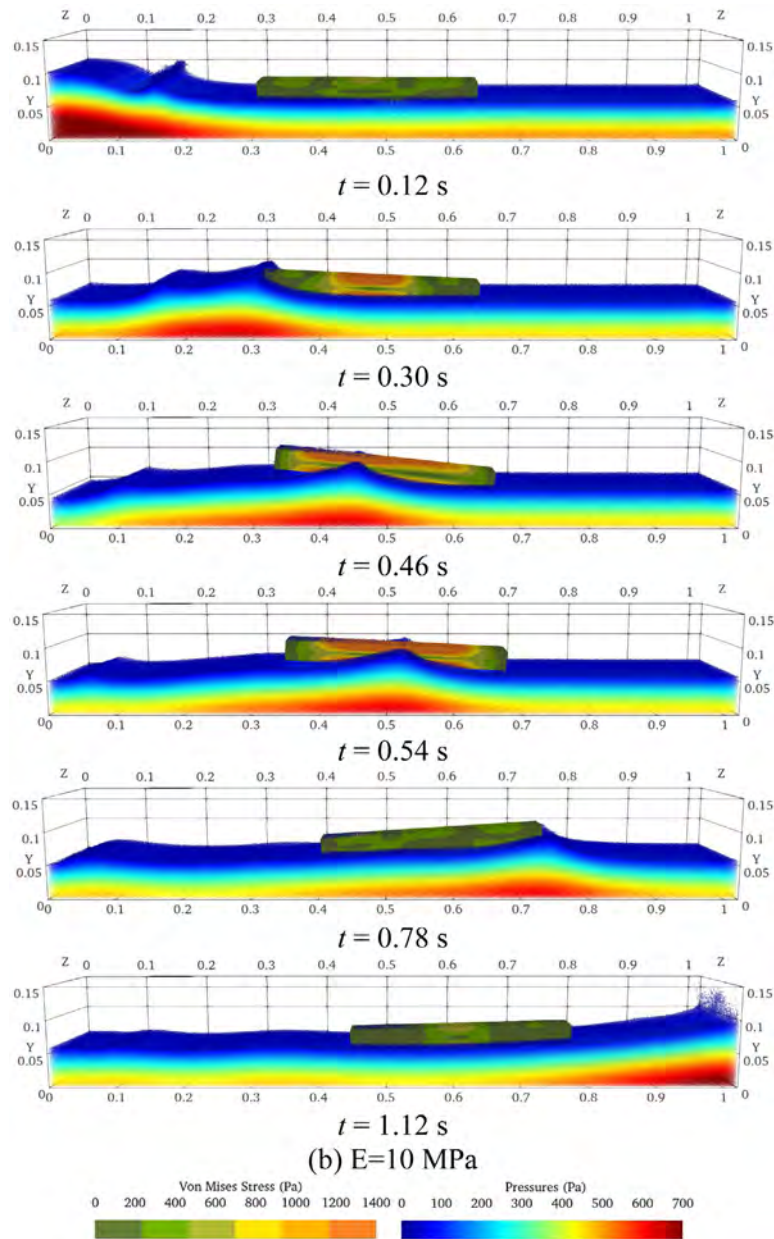


Fig. 18. (continued).

Table 1

The error analysis of the pressure peak.

Points	Experiment data (Pressure, MPa)	$dp = 0.01\text{ m}$ (Pressure, MPa/ ϵ)	$dp = 0.008\text{ m}$ (Pressure, MPa/ ϵ)	$dp = 0.004\text{ m}$ (Pressure, MPa/ ϵ)
A	7.92	9.42/18.9%	10.22/29%	8.82/11%
C	20.27	22.75/12.23%	20.32/0.25%	21.36/5.37%
D	29.99	28.0/6.63%	28.38/5.36%	29.64/1.16%

an unsupported span of 0.495 m, as shown in Fig. 9. The panel falls down with a constant vertical velocity. In the simulation, the particle spacings are $dp = 0.0025\text{ m}$. The total number of particles is 99 398. The time step is set as $\Delta t = 2.5E-5\text{ s}$. 4 CPU cores are used in this case.

Fig. 10 illustrates snapshots of pressure/stress fields at $t = 0.009\text{ s}$, 0.014 s , 0.020 s and 0.026 s , when the panel impacts the still free surface with the velocity of $u = 4.0\text{ m/s}$. Once

the marine panel impacts on the still free surface, the relatively obvious slamming pressure can be observed. During the slamming process, a high-pressure area centered on the contact point between the panel and the free surface is formed. In addition, the range of high-pressure area gradually expands, and the pressure of the contact point gradually increases until the plane completely impacts with the free surface. It can be seen that MPS-FEM coupled solver has provided stable and

reasonable pressure/stress fields all through the instants of slamming phenomenon.

The time history of the deflection at D3 is shown in Fig. 11, when the panel impacts the still free surface with the velocity of $u = 4.0$ m/s. According to the figure, the deflection of D3 almost agrees relatively well with the experiment data by Allen [61] and ISPH-SPH method [47]. Fig. 12 presents the time history of the pressure at P3, when the panel impacts the still free surface with the velocity of $u = 3.0$ m/s. At $t = 0.013$ s, obtained pressure reaches its peak value, about 248 kPa. It can be seen that both the magnitude of pressure peak and the trend of pressure are in good agreement with the experiment [61].

3.3. Dam-breaking wave interacting with a deformable mooring platform

The third validation test for the present MPS–FEM coupled method is dam-breaking wave interacting with a deformable floating platform. The configuration is illustrated in Fig. 13, which is same as the test by Sun [40]. It can be seen that the platform is moored on the bottom of the tank by two cables. It should be noted that the cables are virtual without real particle model, just considering the distance between the bottom of wave flume and the edge of the deformable platform. Then the mooring force acting on the platform obeys Hooke's law with the spring constant of 400 N/m. Besides, the interaction between the cable and the liquid is ignored. During the simulation, the platform may undergo the obvious rigid-body motion and flexible deformation under the wave-induced force and mooring force. The initial particle spacing is set as $dp = 0.002$ m, with the total particle numbers of 17 178. The fluid partition consists of water with density of $\rho = 1000$ kg/m³ and kinematic viscosity of $\nu = 1.01 \times 10^{-6}$ m²/s. Additionally, there is a water damping district to avoid the reflected wave at the end of the tank. As for the structure domain, the deformable floating body is of 0.008 m thickness and 0.1 m length with Young's modulus and density of $E_s = 0.4$ MPa and $\rho_s = 600$ kg/m³. The structural damping is assumed negligible compared to inertial forces. The simulation time is 2 s, and the time step is 0.0002 s. 4 CPU cores are used in this case.

A set of snapshots of the simulation is exhibited in Fig. 14. The water column breaks down and generates a breaking solitary wave from the left, which will impact the platform and cause the rigid-body motion and deformation. It can be seen that the breaking wave can be well captured through the MPS method, and the considerable rigid motion and deformation of the platform can be observed. The pressure is quite smooth and the interaction between the platform and fluid motion is also physically reasonable. Then, the enlarged portions of the simulation result compared with the result of the MPS–DEM coupled method [40] and the platform's stress field are shown in Fig. 15. It can be seen that the motion and deformation of the flexible platform and the motions of the water in numerical simulation agree well with the simulation result from the citation. The present MPS–FEM coupled solver has considerable stability in the reproduction of stress field in the elastic structure and hydrodynamic pressure field.

Moreover, the deformable platform's dimensionless pitch, sway, and surge responses are tracked in Fig. 16, compared with the result of MPS–DEM coupled method [40]. The platform sways around the initial position under the slamming force and mooring force, where the positive motion amplitude is more obvious than that the negative motion due to the dam-breaking wave propagation. It can be seen that the tendency and amplitude of motion responses have a better agreement with the published data [40]. The outcome indicated that the proposed MPS–FEM

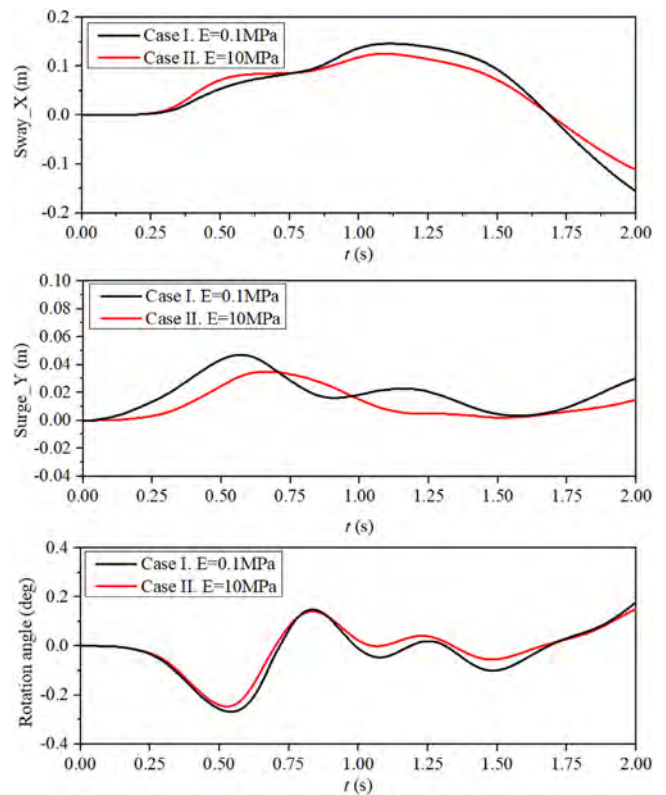


Fig. 19. The interaction between dam-break flow and flexible floating body.

coupled method is suitable for the simulation of wave–structure interaction problems.

4. Numerical simulation

In complicated ocean environments, wave-induced motions and structural distortions are common phenomena under the action of extreme wave loads. In this paper, the proposed MPS–FEM coupled method is applied in three-dimensional wave–structure interaction problems, such as dam-breaking flow impacting a deformable floating body and solitary wave interacting with a flexible ship hull to investigate the hydroelastic responses of floating structures.

4.1. Dam-breaking flow impacting on a deformable floating body

The first test is the interaction between the dam-break wave and three-dimensional floating structure. The numerical model is illustrated in Fig. 17, the geometry of the structure is relatively simple. The simulation starts from the equilibrium state in which the water buoyancy balances out the gravity of the flexible buoyancy tank, the simulation time is 2 s. The computational parameters are shown in Table 2.

A set of snapshots of the simulation of the floating structure of 0.1 MPa is exhibited in Fig. 18(a). The fluid particles are colored by pressure, and von Mises stress colors the structure body. In the simulation, stable and smooth pressure and stress fields are obtained. The water column breaks down and generates a wave to the right, which will impact on the floating structure at around 0.30 s and cause deformation. Then the wave arrives at the stern of the structure at around 0.78 s, and slams on the right wall at around 1.12 s. At last, the reflected wave impacts the floating structure again. During the period, the floating structure presents

Table 2
The computational parameters of the case.

Parameters	Values	Parameters	Values
Fluid density	1000 (kg/m ³)	Structural density	625 (kg/m ³)
Kinematic viscosity	1.01 × 10 ⁻⁶ (m ² /s)	Young's modulus	0.1~10 (MPa)
Particle spacing	0.002 (m)	Element type	Hexahedral solid element
Fluid number	749 541	Element number	40 * 4 * 10
Total number	1 057 902	Poisson's ratio	0.3
CPU cores	10	Time step	0.0005 (s)

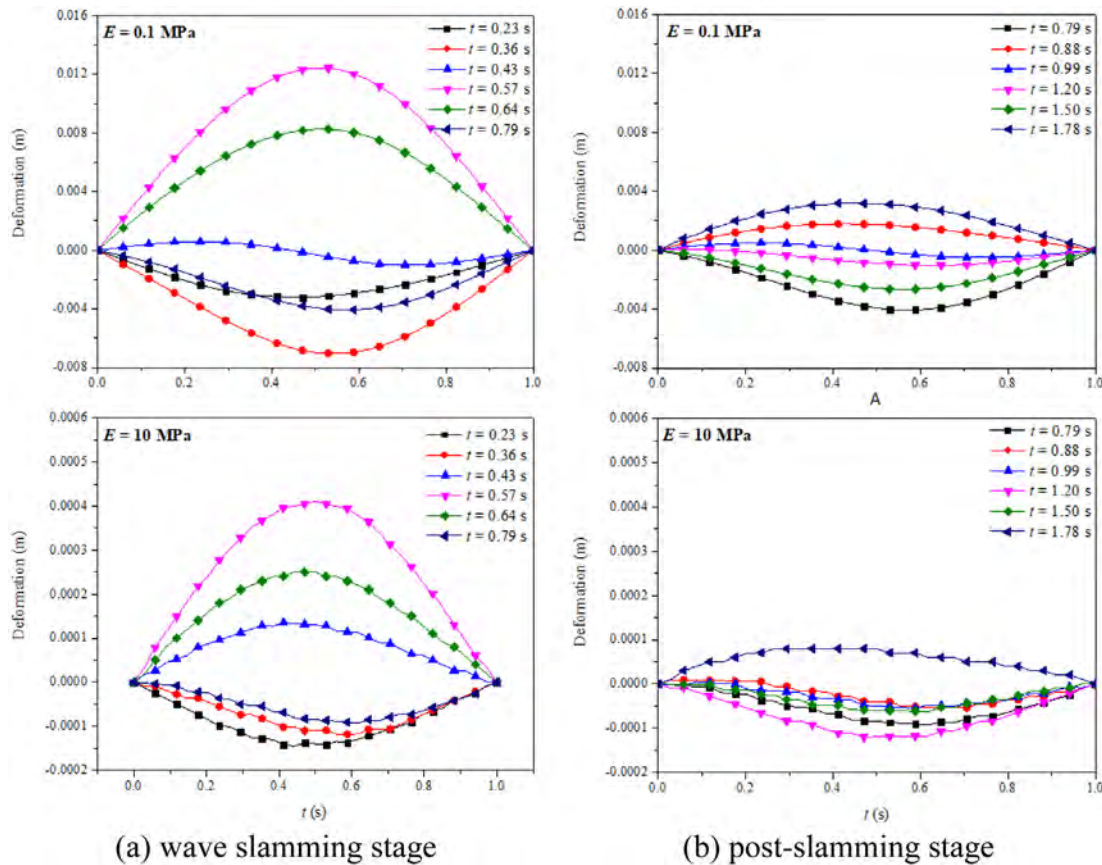


Fig. 20. The deformation of midship section of the platform.

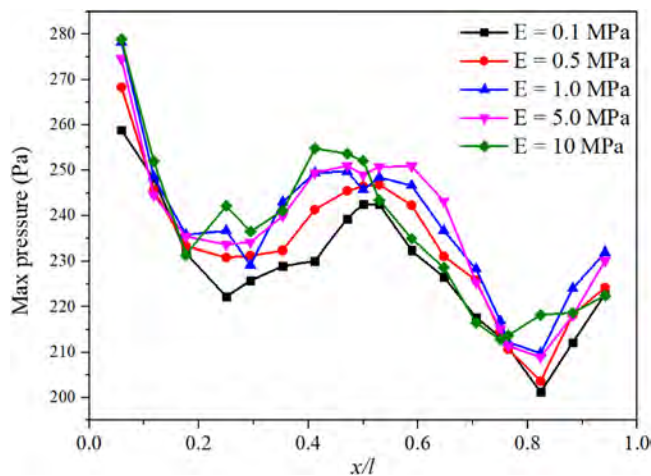


Fig. 21. The maximum pressure along the platform.

under the Young's modulus of 10 MPa are shown as in Fig. 18(b). It can be seen that the more flexible floating structure makes more distinct bending deflection than the one with 10 MPa during the impacting process.

The rigid-body motions of the floating structures under the Young's modulus of 0.1 MPa and 10 MPa are given in Fig. 19, the effect of flexibility is remarkable during the simulation period, especially for the translational motion, the sway and surge motion. This shows that for the interaction problems between the violent flow and flexible structure, the coupling interaction should be considered.

Fig. 20 depicts the deformation of the midship longitudinal section of the platform, the impact process can be divided into two stages, the wave slamming stage during the wave incidence period ($t = 0.20\text{ s} \sim 0.79\text{ s}$) and the post-slamming stage during the wave transmission period (after $t = 0.79\text{ s}$). The deformation in the first stage is mainly caused by wave slamming, while the deformation in the second stage is affected by the natural vibration of the structure. Especially, both ends of the floating structures are regard as fixed. From the figure, it can be seen that the deformation mainly presents hogged deflection and middle sagged deflection. Thus, the first mode is the main response mode

the rigid motion and elastic deformation with the motion of dam-break flow. Then the rigid-body motion and flexible deformation

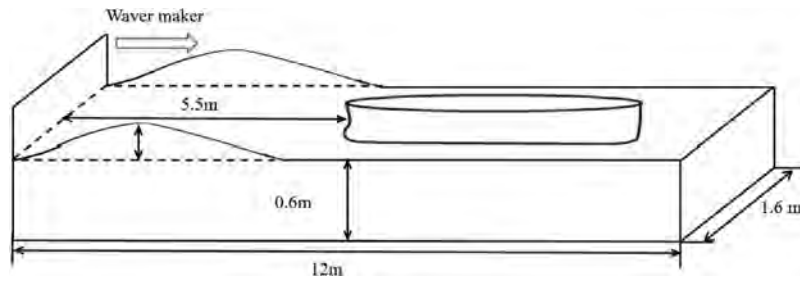
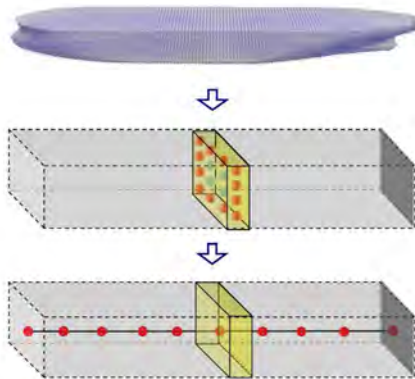


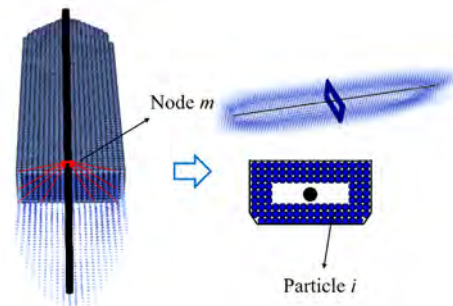
Fig. 22. Geometric model of the numerical wave tank.



(a) The three-view drawing of the ship model



(b) The concepts of the grouping exchange technique



(c) The link between beam nodes and ship boundary particles

Fig. 23. The model of oil tank KVLCC2.

during the impact process under two kinds of stiffness. However, the higher mode is inspired in the case of the Young's modulus of 0.1 MPa. In addition, the deformation in the first stage is more significant than that of the rear stage. The maximum deformation ratio is set as $\Delta = \frac{\delta_{max}}{l}$, where l is the length of the floating structure, and δ_{max} is the maximum deformation. According to the figure, the maximum deformation ratio of Young's modulus of 0.1 MPa is 0.035. While the maximum deformation ratio of the Young's modulus of 10 MPa approaches 0.001 that is the reason for hard to observe the deformation in Fig. 18(b).

According to the aforementioned study, the Young's modulus of the floating platform is one of the most important factors of structural dynamic response. In the rest of this section, five cases with different Young's modulus ($E = 0.1, 0.5, 1, 5$ and 10 MPa) have been tested. During the simulation, a series of pressure probes are located on the bottom of the platform to investigate the bottom slamming. In Fig. 21, the maximum pressure of each probe during the impacting process under the different Young's modulus is shown. It can be seen that the tendency of the maximum pressure along the platform under the different Young's modulus is coincident, like an overturned "ε". The head of the platform is under the maximum pressure, which mostly undertakes the impact of the wave. The maximum pressure gradually reduces along with the platform, while the maximum pressure in

the middle and stern of the platform slightly increases. Moreover, the maximum pressure of the more flexible platform is generally lower than the less flexible platform.

4.2. Solitary wave interacting with a flexible ship hull

In this section, a flexible floating ship model subjected to solitary wave slamming is investigated based on the aforementioned MPS-FEM coupled method. The ship model can be regarded as a nonuniform beam model composed of a series of beam elements. Therefore, the distribution of ship model's mass and inertia moment are calculated first. Then, the accuracy of the generated solitary wave is validated compared with the theoretical solution. At last, the discussion corresponding the flexible floating ship under the solitary wave slamming is conducted.

4.2.1. Geometric model and FEM model

Fig. 22 shows the model of the numerical wave tank together with the ship model. As is shown, the left side of the tank is a piston wave generator used to generate the solitary wave. The initial particle spacing is set as $dp = 0.025$ m, with the total particle numbers of 1 085 209. 10 CPU cores are used in this case. A floating ship model is placed 5.5 m from the piston.

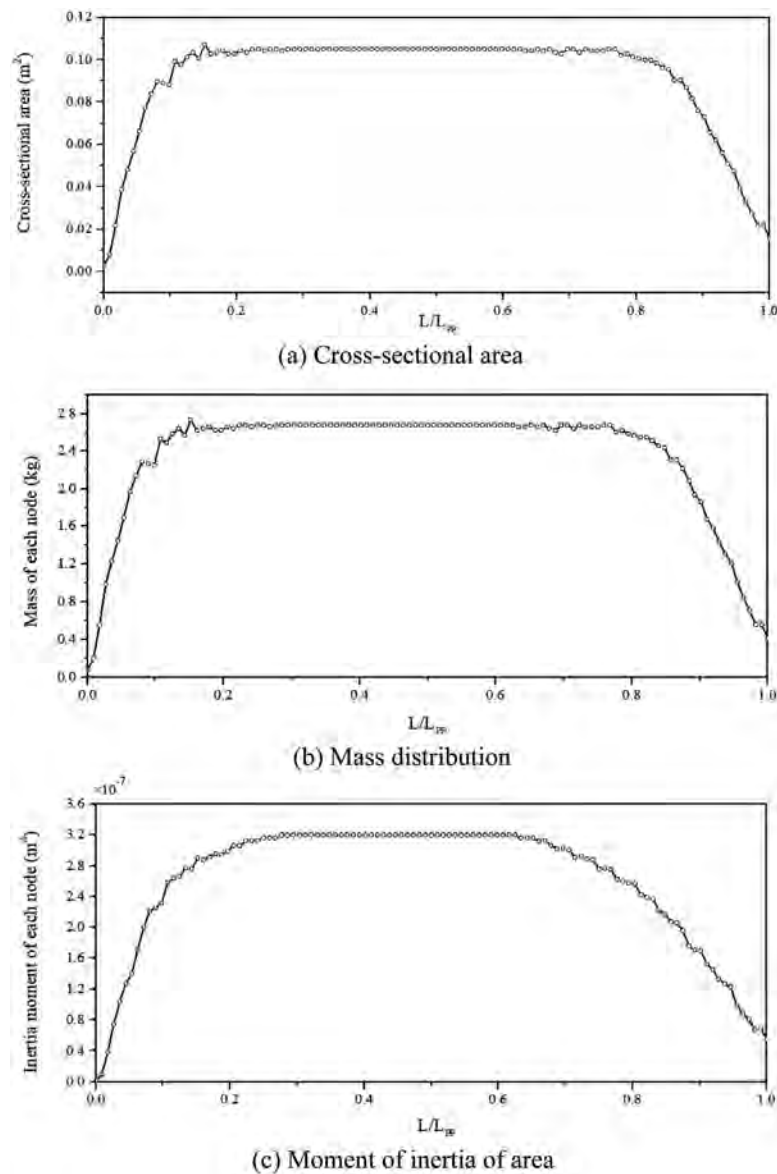


Fig. 24. Cross-sectional area, mass and moment of inertia of area distribution of the model ship.

Table 3

Ship model characteristics.

Principal particulars	Full scale	Ship model
Length between perpendiculars (L [m])	320.0	3.05
Waterline breadth (B [m])	58.0	0.55
Depth (D [m])	30.0	0.29
Draft (d [m])	20.8	0.2
Displacement (∇ [m ³])	312 622	0.27
Scale ratio	105	

In the field of ocean engineering, the geometry model of offshore and ocean structures is usually very complex, which brings a great challenge for particle generating. For instance, Zhu et al. [70] designed a CAD-compatible new body-fitted particle generator for the complex 3D geometry, which can be used for the pre-processing of particle-based methods. In this paper, the ship boundary particles are generated based on the secondary development pre-processing software in the Open-source software DualSPHysics [71]. A 1:105 model of a 320 000-tons oil tank KVLCC2 is constructed in the simulation. The geometric

parameters of ship model are shown in Table 3 [72]. Fig. 23(a) presents the three views of the geometry model, which is created by CATIA. The ship model is dispersed by 16 754 boundary particles, where spacing is the same as the fluid particles. For the dynamics analysis of the ship, the ship model can be dispersed as solid elements, or non-uniform beam model. However, the first choice requires a lot of modeling work and computing resources. By using the non-uniform beam element, the calculation can be greatly simplified. Therefore, in this case, the ship model is regarded as a non-uniform beam comprising 112 beam elements. The grouping exchange technique is considered in this case, the structural particles located within the same section are grouped, as shown in Fig. 23(b). According to Fig. 23(c), the ship boundary particles are connected to the nodes on the beam elements. Consequently, the beam deformations are imparted on to the ship hull.

However, some physical parameters of the non-uniform beam are difficult to determine, such as cross-sectional area and cross-sectional moment of inertia, which are not a constant and vary along the non-uniform beam. According to the draft and the hull thickness of the ship model, the density of the ship model is set

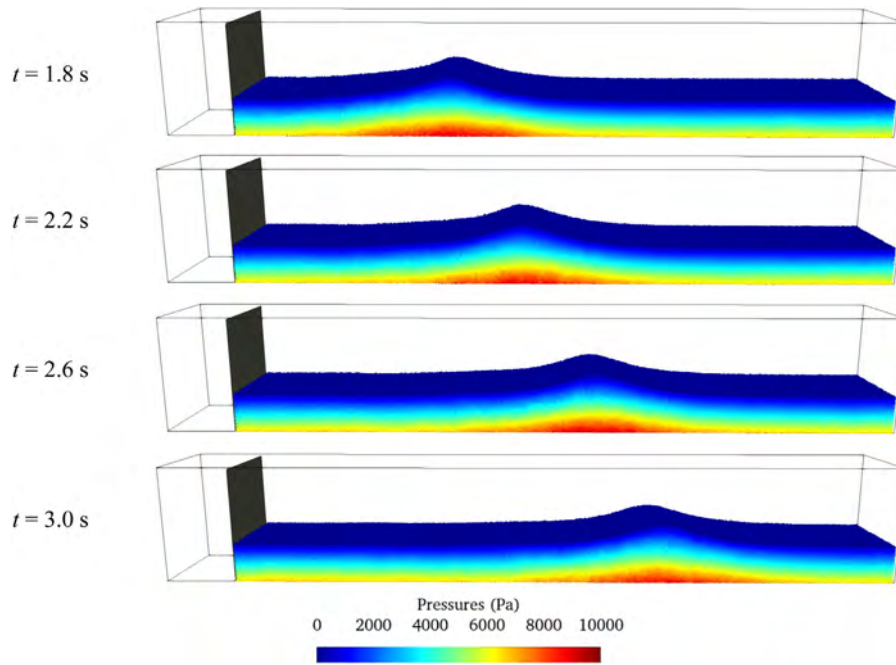


Fig. 25. The solitary wave propagation process in the numerical tank.

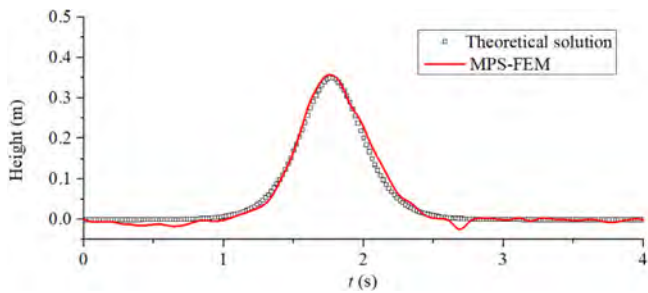


Fig. 26. The wave evolution in front of the ship model.

as 945 kg/m^3 . Then the ship model's mass distribution, the cross-sectional area and the 2nd moment of area can be calculated through the ship boundary particle distribution, which can be expressed as follows,

$$A_m = \sum_{i=1} A_i \tag{25}$$

$$M_m = \rho_s A_m, \quad M_s = \rho_s \int A dl \tag{26}$$

$$I_m = \int y^2 dA = \sum_{i=1} y_i^2 \cdot A_i \tag{27}$$

where A , M , I denote the cross-sectional area, the mass and the 2nd moment of area. The subscript i , m and S present the ship boundary particle i , the non-uniform beam node m , and the ship model S . Fig. 24 shows the resultant cross-sectional area, mass and 2nd moment distribution of the model ship. By integrating the curve in Fig. 24(b), the total mass of the ship model is 265.4 kg, which is consistent with the data in Table 3. It can prove that this statistical method is effective. The Young's modulus of the ship model is set as 0.04 MPa, which is relatively small, so that the deformation of structure can be clearly observed. The total mass of the ship is distributed on the beam elements as lumped masses. The structural damping is assumed negligible.

4.2.2. Numerical wave generations

It is of importance to examine the accuracy of the generated solitary wave. According to the Korteweg–de Vries (KdV) equation, the profile of the solitary wave can be expressed as follows [73]:

$$\eta = A \text{sech}^2(k(x - ct)) \tag{28}$$

$$k = \sqrt{3A/4H^3} \tag{29}$$

$$c = \sqrt{g(A + H)} \tag{30}$$

where A is the water height, also is the wave amplitude for solitary wave. H , x and c denote the water depth, the horizontal coordinate and the wave speed. In this paper, the solitary wave is generated by a piston-type wavemaker, whose motion was described by Goring [74]. The speed of the wavemaker is formulated as:

$$U(t) = \frac{dX(t)}{dt} = \frac{c\eta}{H + \eta} = \frac{cA \text{sech}^2(k(X - ct))}{H + A \text{sech}^2(k(X - ct))} \tag{31}$$

Thus, the position of the wavemaker at time t can be expressed as:

$$X(t) = \frac{A}{kH} \tanh(k(ct - X)) \tag{32}$$

Therefore, the stroke of the wave maker can be obtained from the above equation, written as,

$$S = X(+\infty) - X(-\infty) = \sqrt{16AH/3} \tag{33}$$

The verification is conducted in the numerical wave tank without the ship model. The solitary wave, with wave amplitude of $A/H = 0.6$, is adopted in the simulations. Fig. 25 shows the solitary wave propagation process in the numerical tank. It can be seen that the pressure of the fluid field remains smooth during the whole process of wave propagation, and no obvious attenuation of the wave crest can be observed. Fig. 26 shows the results of numerical wave elevation versus the theoretical solution. The wave elevation is measured near the location of the ship bow to determine the reliability of the generated waves. The numerical

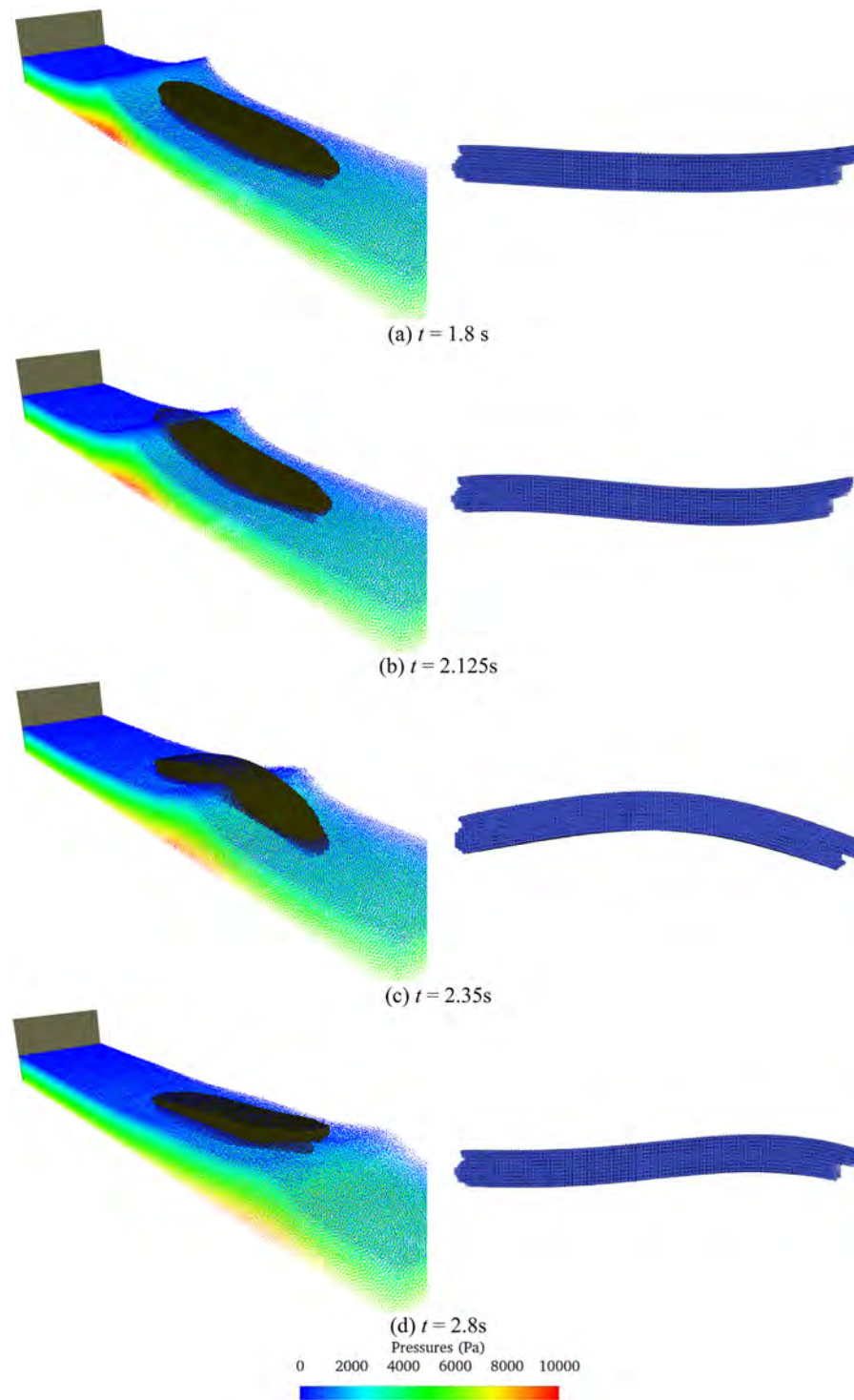


Fig. 27. The free surface profiles at typical time instants.

free surface elevation is in good agreement with the analytical solution.

4.2.3. Results and discussion

The motion of the flexible ship model subjected to solitary wave slamming is studied. The free surface profiles and the pressure distribution of the fluid field, and the vibration of the ship hull at typical time instants are exhibited in Fig. 27. A lower stiffness of ship model is chosen to test the capability of

present solver. Consequently, the amplitude of the deformation is significantly larger than the normal ship structure. As can be seen in the figure, the pressure field is smooth and stable without any pressure oscillation. The wave impacts onto the ship bow at around 1.8 s. The ship bow presents the upward tendency. Then the wave crest touches the bow, the wave crest is higher than the bow, the phenomenon green water can be observed, the ship model presents high-order modes. As the wave propagating along the ship hull and arriving at the midship, the ship model

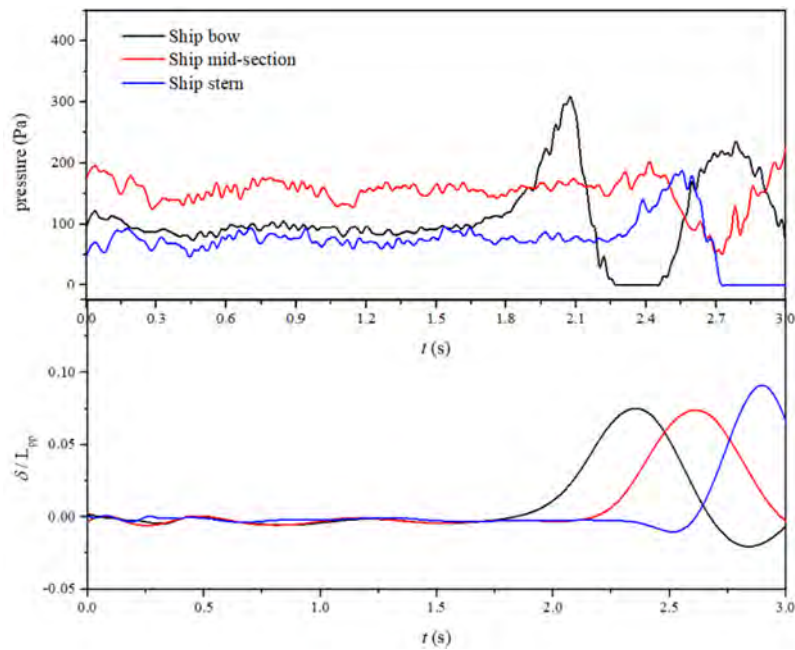


Fig. 28. The time histories of impact pressure and ship deflection.

has hogging deformation. At around 2.8 s, the wave propagates to the stern, the ship stern is lifted up, the ship model presents high-order modes again.

Finally, the pressure of the ship bow, mid-section and stern, together with the corresponding dimensionless deflection are exhibited in Fig. 28. During the developing process of the impact solitary wave, the pressure is almost stable with slight oscillation in first 0.5 s. The ship model mostly remains at the same position at this time. It can be proved that the hydrostatic load calculated by the present solver is accurate and stable to support the ship's weight. And due to the non-uniform section, initial hydrostatic pressure is different. As the impact wave propagating along with the ship model, the time history of impact pressures is consistent with the deflections of corresponding position.

In this section, a series of qualitative analyses show that present solver can provide reasonable predictions for the simulation of wave–ship interaction. However, a more quantitative analysis would be required to further verify the reliability of this work by comparing the results against published experimental or numerical data.

5. Conclusions

In this paper, the coupling MPS–FEM method is applied to simulate the hydroelastic response of floating structures in waves. Especially, a rigid–flexible coupling strategy based on MPS–FEM coupled method is proposed in this paper for the deformable floating structures. In the MPS–FEM coupled solver, according to the choice of structural element, appropriate data transformation schemes are adopted on the fluid–structure interface. In this paper, the grouping exchange technique is proposed, which is applied on the interface of particle model–beam element. On the interface of particle model–solid element, the Shape Function Based Interpolation Technique (SFBI) was applied.

The reliability of the present method is validated by the cases of hydroelastic slamming of an elastic wedge, hydroelastic slamming of the marine panel and dam-break wave impacting on a mooring platform. The capable of present solver in simulating the rigid-body motion coupled with elastic deformation is

investigated. The pressure/stress fields obtained is stable and reasonable through MPS–FEM coupled solver. The numerical results obtained are in good agreement with published data. Afterwards, the coupling solver is also applied for the three-dimensional wave–structure problems including the cases of deformable floating platform slamming in waves and a complexity ship model subjected to solitary wave impacting, the outcome indicates that present solver is of good potential in practical engineering application.

In this work, a series of qualitative analyses show that present solver can provide reasonable predictions for the simulation of wave–structure problems. However, a more quantitative analysis would be required to further verify the reliability of this work. In addition, the ship hull model is dispersed as non-uniform beam elements to save computation resource. However, local deformation in the hull model induced by the local pressure will be ignored in this way. In the future, a refined discrete form will be applied on the ship hull model for a more detailed dynamic response analysis. Besides, the fluid force acting on the object includes the surface pressure and the viscous fluid shear force. However, the viscous fluid shear force was excluded in present paper. In further work, the viscous fluid shear force will be included in the rigid body dynamic equations. Finally, more refined schemes will be applied in MPS method, such as the particle shifting technique [75,76] and high-order source terms [77].

Declaration of competing interest

The authors declare the following financial interests/personal relationships which may be considered as potential competing interests: Decheng Wan reports financial support was provided by Shanghai Jiao Tong University.

Data availability

The data that support the findings of this study are available from the corresponding author upon reasonable request.

Acknowledgments

This work was supported by National Natural Science Foundation of China (Grant No. 51879159, 52131102), National Key Research and Development Program of China (2019YFB1704200), to which the authors are most grateful.

References

- [1] T.E. Tezduyar, M. Behr, J. Liou, A new strategy for finite element computations involving moving boundaries and interfaces-The deforming-spatial-domain/space-time procedure: I. The concept and the preliminary numerical tests, *Comput. Methods Appl. Mech. Engrg.* 94 (3) (1992) 339–351.
- [2] C. Peskin, The immersed boundary method, *Acta Numer.* 011 (2002) 479–517.
- [3] S. Ghosh, J.M. Stockie, Numerical simulations of particle sedimentation using the immersed boundary method, *Commun. Comput. Phys.* 18 (2015) 380–416.
- [4] D.W. Qi, Lattice-Boltzmann simulations of particles in non-zero-Reynolds-number flows, *J. Fluid Mech.* 385 (1999) 41–62.
- [5] B. Yang, S. Chen, C. Cao, Z. Liu, C. Zheng, Lattice Boltzmann simulation of two cold particles settling in Newtonian fluid with thermal convection, *Int. J. Heat Mass Transfer* 93 (2016) 477–490.
- [6] Z.R. Shen, P.M. Carrica, D.C. Wan, Ship motions of KCS in head waves with rotating propeller using overset grid method, in: *Proceedings of the 33rd International Conference on Ocean, Offshore and Arctic Engineering*, OMAE, San Francisco, 2014, pp. 2014–23657.
- [7] P.A. Lakshminarayanan, P. Temarel, Application of CFD and FEA coupling to predict dynamic behaviour of a flexible barge in regular head waves, *Mar. Struct.* 65 (2019) 308–325.
- [8] P.A. Lakshminarayanan, P. Temarel, Application of two-way partitioned method for predicting the wave-induced loads of a flexible containership, *Appl. Ocean Res.* 96 (2020).
- [9] T. Wick, Monolithic fluid-structure interaction problems in arbitrary Lagrangian Eulerian coordinates with the deal. II library, *Arch. Numer. Softw.* 1 (1) (2013) 1–19.
- [10] X. Wen, W.W. Zhao, D.C. Wan, A multiphase MPS method for bubbly flows with complex interfaces, *Ocean Eng.* 238 (2021) 109743.
- [11] Y. Shimizu, A. Khayyer, H. Gotoh, K. Nagashima, An enhanced multiphase ISPH-based method for accurate modeling of oil spill, *Coast. Eng. J.* 62 (2020) 625–646.
- [12] L.B. Lucy, A numerical approach to the testing of the fission hypothesis, *Astron. J.* 82 (1977) 1013–1024.
- [13] S. Koshizuka, Y. Oka, Moving-particle semi-implicit method for fragmentation of incompressible fluid, *Nucl. Sci. Eng.* 123 (3) (1996) 421–434.
- [14] D. Sulsky, Z. Chen, H.L. Schreyer, Particle method for history-dependent materials, *Comput. Methods Appl. Mech. Engrg.* 118 (1–2) (1994) 179–196.
- [15] M. Gomez-Gesteira, R.A. Dalrymple, Using a three-dimensional smoothed particle hydrodynamics method for wave impact on a tall structure, *J. Waterw. Port Coast. Ocean Eng.* 130 (2) (2004) 63–69.
- [16] Z.Y. Tang, Y.L. Zhang, D.C. Wan, Multi-resolution MPS method for free surface flows, *Int. J. Comput. Methods* 13 (4) (2016) 1–17.
- [17] X. Chen, D.C. Wan, GPU accelerated MPS method for large-scale 3-D violent free surface flows, *Ocean Eng.* 171 (2019) 677–694.
- [18] K. Gong, H. Liu, B.L. Wang, Water entry of a wedge based on SPH model with an improved boundary treatment, *J. Hydrodyn.* 21 (6) (2009) 750–757.
- [19] G. Oger, D.L. Touzé, B. Alessandrini, P. Maruwski, A new parallelized 3d sph model: resolution of water entry problems and scalability study, *Ercofac Bull.* 76 (1) (2008) 145–149.
- [20] P.N. Sun, F.R. Ming, A.M. Zhang, Numerical simulation of interactions between free surface and rigid body using a robust SPH method, *Ocean Eng.* 98 (2015) 32–49.
- [21] B.H. Lee, S.M. Jeong, S.C. Hwang, J.C. Park, M.H. Kim, A particle simulation of 2-D vessel motions interacting with liquid-sloshing cargo, *CMES Comput. Model. Eng. Sci.* 91 (1) (2013) 43–63.
- [22] Y.X. Zhang, D.C. Wan, Comparative study of MPS method and level-set method for sloshing flows, *J. Hydrodyn.* 26 (4) (2014) 577–585.
- [23] H.Z. Li, Z.Y. Tang, D.C. Wan, Application of GPU acceleration techniques in 3D violent free surface flows, *Ocean Eng.* 34 (5) (2016) 20–29, (in Chinese).
- [24] F.Z. Xie, W.W. Zhao, D.C. Wan, CFD simulations of three-dimensional violent sloshing flows in tanks based on MPS and GPU, *J. Hydrodyn.* 32 (5) (2020) 672–683.
- [25] M. Sueyoshi, M. Kashiwagi, S. Naito, Numerical simulation of wave-induced nonlinear motions of a two-dimensional floating body by the moving particle semi-implicit method, *J. Mar. Sci. Technol.* 13 (2) (2008) 85–94.
- [26] K. Shibata, S. Koshizuka, M. Sakai, K. Tanizawa, Lagrangian simulations of ship wave interactions in rough seas, *Ocean Eng.* 42 (2012) 13–25.
- [27] K. Guo, P.N. Sun, X.Y. Cao, X. Huang, A 3-D SPH model for simulating water flooding of a damaged floating structure, *J. Hydrodyn.* 29 (5) (2017) 831–844.
- [28] K. Kawamura, H. Hashimoto, A. Matsuda, D. Terada, SPH simulation of ship behaviour in severe water-shipping situations, *Ocean Eng.* 120 (1) (2016) 220–229.
- [29] X.Y. Ni, W.B. Feng, S.C. Huang, Z.J. Hu, Y. Liu, An SPH wave-current flume using open boundary conditions, *J. Hydrodyn.* 32 (3) (2019) 536–547.
- [30] M. Liu, Z. Zhang, Smoothed particle hydrodynamics (SPH) for modeling fluid-structure interactions, *Sci. China Phys. Mech. Astron.* 62 (2019).
- [31] A. Khayyer, H. Gotoh, Y. Shimizu, Y. Nishijima, A 3D Lagrangian mesh-free projection-based solver for hydroelastic fluid-structure interactions, *J. Fluids Struct.* 105 (2021) 103342.
- [32] N. Mitsume, S. Yoshimura, K. Murotani, T. Yamada, Improved MPS-FE fluid-structure interaction coupled method with MPS polygon wall boundary model, *Comput. Model. Eng. Sci.* 101 (4) (2014) 229–247.
- [33] Y.L. Zhang, X. Chen, D.C. Wan, An MPS-FEM coupled method for the comparative study of liquid sloshing flows interacting with rigid and elastic baffles, *Appl. Math. Mech.* 37 (12) (2016) 1359–1377.
- [34] Z.M. Zheng, G.T. Duan, N. Mitsume, S.H. Chen, S. Yoshimura, A novel ghost cell boundary model for the explicit moving particle simulation method in two dimensions, *Comput. Mech.* 66 (4) (2020) 87–102.
- [35] Z.M. Zheng, G.T. Duan, N. Mitsume, S.H. Chen, S. Yoshimura, An explicit MPS/FEM coupling algorithm for three-dimensional fluid-structure interaction analysis, *Eng. Anal. Bound. Elem.* 121 (2020) 192–206.
- [36] G.Y. Zhang, W.W. Zhao, D.C. Wan, Partitioned MPS-FEM method for free-surface flows interacting with deformable structures, *Appl. Ocean Res.* 114 (2021) 102775.
- [37] Q. Yang, V. Jones, L. McCue, Free-surface flow interactions with deformable structures using an SPH-FEM model, *Ocean Eng.* 55 (2012) 136–147.
- [38] G. Fourey, C. Hermange, D.L. Touzé, G. Oger, An efficient FSI coupling strategy between smoothed particle hydrodynamics and finite element methods, *Comput. Phys. Comm.* 217 (2017) 66–81.
- [39] C. Hermange, G. Oger, Y.L. Chenadec, D.L. Touzé, A 3D SPH-FE coupling for FSI problems and its application to tire hydroplaning simulations on rough ground, *Comput. Methods Appl. Mech. Engrg.* 355 (2019) 558–590.
- [40] Y.J. Sun, G. Xi, Z.G. Sun, A fully Lagrangian method for fluid-structure interaction problems with deformable floating structure, *J. Fluids Struct.* 90 (2019) 379–395.
- [41] F.Z. Xie, W.W. Zhao, D.C. Wan, MPS-DEM coupling method for interaction between fluid and thin elastic structures, *Ocean Eng.* 236 (2021) 109449.
- [42] Z. Sun, K. Djidjeli, J.T. Xing, F. Cheng, Coupled MPS-modal superposition method for 2D nonlinear fluid-structure interaction problems with free surface, *J. Fluids Struct.* 61 (2016) 295–323.
- [43] Z. Sun, G.Y. Zhang, Z. Zong, K. Djidjeli, J.T. Xing, Numerical analysis of violent hydroelastic problems based on a mixed MPS-mode superposition method, *Ocean Eng.* 179 (2019) 285–297.
- [44] J. O'Connor, B.D. Rogers, A fluid-structure interaction model for free-surface flows and flexible structures using smoothed particle hydrodynamics on a GPU, *J. Fluids Struct.* 104 (2021) 103312.
- [45] P.N. Sun, D.L. Touzé, G. Oger, An accurate FSI-SPH modeling of challenging fluid-structure interaction problems in two and three dimensions, *Ocean Eng.* 221 (2021) 108552.
- [46] L. Zhan, C. Peng, B. Zhang, A stabilized TL-WC SPH approach with GPU acceleration for three-dimensional fluid-structure interaction, *J. Fluids Struct.* 86 (2019) 329–353.
- [47] A. Khayyer, H. Gotoh, H. Falahaty, Y. Shimizu, An enhanced ISPH-SPH coupled method for simulation of incompressible fluid-elastic structure interactions, *Comput. Phys. Comm.* 232 (2018) 139–164.
- [48] A. Khayyer, N. Tsuruta, Y. Shimizu, H. Gotoh, Multi-resolution MPS for incompressible fluid-elastic structure interactions in ocean engineering, *Appl. Ocean Res.* 82 (2019) 397–414.
- [49] C. Zhang, M. Rezavand, X.Y. Hu, A multi-resolution SPH method for fluid-structure interactions, *J. Comput. Phys.* 429 (2021) 110028.
- [50] P.N. Sun, D. Le Touzé, A.M. Zhang, Study of a complex fluid-structure dam-breaking benchmark problem using a multi-phase SPH method with APR, *Eng. Anal. Bound. Elem.* 104 (2019) 240–258.
- [51] A. Khayyer, Y. Shimizu, H. Gotoh, S. Hattori, Multi-resolution ISPH-SPH for accurate and efficient simulation of hydroelastic fluid-structure interactions in ocean engineering, *Ocean Eng.* 226 (2021) 108652.
- [52] T. Long, C. Huang, D. Hu, M.B. Liu, Coupling edge-based smoothed finite element method with smoothed particle hydrodynamics for fluid structure interaction problems, *Ocean Eng.* 225 (2021) 108772.
- [53] A. Khayyer, Y. Shimizu, H. Gotoh, K. Nagashima, A coupled incompressible SPH-Hamiltonian SPH solver for hydroelastic FSI corresponding to composite structures, *Appl. Math. Model.* 94 (2021) 242–271.

- [54] H. Gotoh, A. Khayyer, Y. Shimizu, Entirely Lagrangian meshfree computational methods for hydroelastic fluid–structure interactions in ocean engineering—Reliability, adaptivity and generality, *Appl. Ocean Res.* 115 (2021) 102822.
- [55] Y.X. Zhang, D.C. Wan, Apply MPS method to simulate liquid sloshing in LNG tank, in: *Proceedings of 22nd International Offshore and Polar Engineering Conference*, June 17–23 (2012), pp. 381–391.
- [56] Z.Y. Tang, D.C. Wan, Numerical simulation of impinging jet flows by modified MPS method, *Eng. Comput.* 32 (4) (2015) 1153–1171.
- [57] Y.L. Zhang, D.C. Wan, MPS-FEM coupled method for sloshing flows in an elastic tank, *Ocean Eng.* 152 (2018) 416–427.
- [58] C.P. Rao, D.C. Wan, Numerical study of the wave-induced slamming force on the elastic plate based on MPS-FEM coupled method, *J. Hydrodyn.* 30 (1) (2018) 70–78.
- [59] G.Y. Zhang, X. Chen, D.C. Wan, MPS-FEM coupled method for study of wave-structure interaction, *J. Mar. Sci. Appl.* 18 (4) (2019) 387–399.
- [60] Y.M. Scolan, Hydroelastic behaviour of a conical shell impacting on a quiescent-free surface of an incompressible liquid, *J. Sound Vib.* 277 (2004) 163–203.
- [61] T. Allen, *Mechanics of Flexible Composite Hull Panels Subjected to Water Impacts* (Ph.D. thesis), University of Auckland, 2013.
- [62] M. Tanaka, T. Masunaga, Stabilization and smoothing of pressure in MPS method by quasi-compressibility, *J. Comput. Phys.* 229 (11) (2010) 4279–4290.
- [63] B.H. Lee, J.C. Park, M.H. Kim, S.C. Hwang, Step-by-step improvement of mps method in simulating violent free-surface motions and impact-loads, *Comput. Methods Appl. Mech. Eng.* 200 (9–12) (2011) 1113–1125.
- [64] A. Khayyer, H. Gotoh, S.D. Shao, Enhanced predictions of wave impact pressure by improved incompressible SPH methods, *Appl. Ocean Res.* 31 (2) (2009) 111–131.
- [65] S.C. Hwang, A. Khayyer, H. Gotoh, J.C. Park, Development of a fully Lagrangian MPS-based coupled method for simulation of fluid–structure interaction problems, *J. Fluids Struct.* 50 (2) (2014) 497–511.
- [66] S. Koshizuka, A. Nobe, Y. Oka, Numerical analysis of breaking waves using the moving particle semi-implicit method, *Internat. J. Numer. Methods Fluids* 26 (7) (1998) 751–769.
- [67] S. Marrone, B. Bouscasse, A. Colagrossi, M. Antuono, Study of ship wave breaking patterns using 3D parallel SPH simulations, *Comput. Fluids* 69 (2012) 54–66.
- [68] N.M. Newmark, A method of computation for structural dynamics, *J. Eng. Mech. Div.* 85 (3) (1959) 67–94.
- [69] S.C. Hwang, J.C. Park, H. Gotoh, A. Khayyer, K.J. Kang, Numerical simulations of sloshing flows with elastic baffles by using a particle-based fluid–structure interaction analysis method, *Ocean Eng.* 118 (2016) 227–241.
- [70] Y. Zhu, C. Zhang, Y. Yu, X. Hu, A CAD-compatible body-fitted particle generator for arbitrarily complex geometry and its application to wave-structure interaction, *J. Hydrodyn.* 33 (2) (2021) 195–206.
- [71] A.J.C. Crespo, J.M. Domínguez, B.D. Rogers, M. Gómez-Gesteira, S. Longshaw, R. Canelas, R. Vacondio, A. Barreiro, O. García-Feal, Dual-SPHysics: Open-source parallel CFD solver based on smoothed particle hydrodynamics (SPH), *Comput. Phys. Comm.* 187 (2015) 204–216.
- [72] http://www.simman2008.dk/KVLCC/KVLCC2/kvlcc2_geometry.html.
- [73] D.J. Korteweg, G. de Vries, On the change of form of long waves advancing in a rectangular canal and on a new type of long stationary waves, *Phil. Mag.* 36 (1895) 422–443.
- [74] D.G. Goring, *Tsunamis—the Propagation of Long Waves onto a Shelf* (Ph.D. thesis), California Institute of Technology, Pasadena, California, USA, 1978.
- [75] S.J. Lind, R. Xu, P.K. Stansby, B.D. Rogers, Incompressible smoothed particle hydrodynamics for free-surface flows: A generalized diffusion-based algorithm for stability and validations for impulsive flows and propagating waves, *J. Comput. Phys.* 231 (2012) 1499–1523.
- [76] A. Khayyer, H. Gotoh, Y. Shimizu, Comparative study on accuracy and conservation properties of two particle regularization schemes and proposal of an optimized particle shifting scheme in ISPH context, *J. Comput. Phys.* 332 (2017) 236–256.
- [77] A. Khayyer, H. Gotoh, Modified moving particle semi-implicit methods for the prediction of 2D wave impact pressure, *Coast. Eng.* 56 (2009) 419–440.